# Feasibility of geothermal energy in the Belgian deep railway tunnels: case of the Liefkenshoek tunnel

**Auteur :** Noubi Tchoupe, Audrey Shelsi
**Promoteur(s) :** Dewallef, Pierre
**Faculté :** Faculté des Sciences appliquées
**Diplôme :** Master : ingénieur civil en génie de l'énergie à finalité spécialisée en Energy Conversion
**Année académique :** 2024-2025
**URI/URL :** http://hdl.handle.net/2268.2/24564

**University of Liège**
Faculty of Applied Sciences

# Feasibility of geothermal energy in the Belgian deep railway tunnels: Case of the Liefkenshoek tunnel

NOUBI TCHOUPE Audrey Shelsi

Thesis presented to obtain the degree of:
**Master of Science in Energy Engineering**

**Thesis Supervisors**

DEWALLEF Pierre
DE PAUW Bart

**Jury Members**

LEMORT Vincent
BERTRAND François

Academic year: **2024 - 2025**

# Acknowledgements

I thank Providence for the health and strength that allowed me to overcome every challenge.
I want to express my sincere gratitude to Mr. Pierre DEWALLEF, Mr. François BERTRAND, Mr. Bart DE PAUW, and Ms. Natalia KOZLOWSKA for their guidance and support throughout this work.
I also extend my thanks to the University of Liège, and in particular to the laboratory of thermodynamics, for the rigorous and high-quality education I received.
Finally, I thank my family and friends for their constant support throughout this journey.

# Abstract

The energy sector is undergoing a major transition aimed at reducing or eliminating fossil fuels in favour of renewable sources such as solar, biomass, wind and geothermal energy. In the case of geothermal energy, the use of geostructures is expanding due to the possibility of thermally activating them by integrating heat exchangers; thermally activated tunnels (energy tunnels) are a representative application. Thermal activation of tunnels offers strong potential owing to their large contact area with the ground, an essential advantage underpinning this feasibility study. This work assesses the technical and economic feasibility of thermally activating the Liefkenshoek railway tunnel (Belgium) by evaluating both the exploitable geothermal potential and the project's profitability. To this end, an analytical heat transfer model was developed and tested under different conditions. The analysis also accounts for variations in several key parameters: the inlet temperature of the heat transfer fluid, its flow rate through the exchanger, and the air temperature inside the tunnel. The results indicate that water saturated sand yields the highest geothermal potential, and under specific conditions, an exploitable potential of $27\,\mathrm{W/m^2}$ was identified. Finally, the economic assessment indicates that, under suitable operating conditions, the project is economically viable, with the heat production cost remaining significantly lower than the typical selling price observed on district heating networks. This work, therefore, contributes to the valorisation of existing infrastructure within the energy transition and recommends the systematic integration of thermal activation in future tunnel construction projects.

# Contents

# List of Figures

# List of Symbols

$T_{\text{ground}}$: Ground temperature [°C]

$T_{\text{air}}$: Tunnel air temperature [°C]

$T_{\text{s}}$: Surface temperature of the heat exchanger pipe [°C]

$T_{\text{in,fluid}}$: Inlet temperature of the heat transfer fluid [°C]

$T_{\text{out,fluid}}$: Outlet temperature of the heat transfer fluid [°C]

$T_{\text{out,heatpump}}$: Outlet temperature of the heat pump [°C]

$k$: Thermal conductivity [W/(m K)]

$\rho$: Density [kg/m$^3$]

$c$: Specific heat capacity [J/(kg K)]

$\alpha$: Thermal diffusivity [m$^2$/s]

$R_{\text{ground}}$: Thermal resistance of the ground [K/W]

$R_{\text{concrete,in}}$: Thermal resistance of the inner concrete layer [K/W]

$R_{\text{concrete,out}}$: Thermal resistance of the outer concrete layer [K/W]

$R_{\text{conv,air}}$: Convective resistance of tunnel air [K/W]

$h_{\text{conv}}$: Convective heat transfer coefficient [W/(m$^2$ K)]

$D_{\text{in}}, D_{\text{out}}$: Inner and outer tunnel diameters [m]

$L_r$: Axial length of the tunnel ring [m]

$L_p$: Length of Pe-Xa pipe [m]

$d_e$: Outer diameter of Pe-Xa pipe [m]

$e_p$: Wall thickness of Pe-Xa pipe [m]

$p$: Position of the pipe in concrete [m]

$A_s$: Active heat exchange surface area [m$^2$]

$q^*$: Dimensionless extracted heat [-]

$q^*_{\text{ss}}$: Steady-state dimensionless heat [-]

$Fo$: Fourier number [-]

$L_c$: Characteristic length [m]

$\dot{m}_{\text{fluid}}$: Mass flow rate of the heat transfer fluid [kg/s]

$\Delta T_{\text{lm}}$: Log mean temperature difference [K]

$A_{\text{lat}}$: Lateral surface area of the pipe [$m^2$]

$\text{COP}_{\text{Carnot}}$: Carnot coefficient of performance [-]

# List of Tables

# Chapter 1

# Introduction

## 1.1 Context

The energy sector is undergoing a transition that relies on changes in the distribution of various primary energy sources used in the economy to reduce or eliminate the share of fossil fuels, namely coal, oil, and natural gas [1]. The legal framework supporting this energy transition is the 2015 Paris Agreement under the COP, which, in Article 2, sets the goal of limiting the global average temperature rise to below 2°C compared to preindustrial levels [2]. Furthermore, each country is responsible for defining an energy policy that aligns with this goal. According to IRENA [3], the six main areas where European energy policies and decisions must be made and implemented are: exploiting the strong synergies between energy efficiency and renewable energy; designing an electricity grid in which renewable energy plays a significant role; increasing the use of electricity in transport, buildings, and industry; supporting innovation throughout the system; aligning socioeconomic structures and investments with the transition; and ensuring fair redistribution of the costs and benefits associated with the transition. Regarding renewable energy, there has been a significant deployment in recent years, and in 2023 it accounted for 24.5 % of the European Union's energy consumption [4]. In Europe in general and Belgium in particular, renewable energy sources are: wind energy, hydropower, solar energy, geothermal energy, chemical energy, and biomass [5]. It should be noted that various technologies for exploiting each of these sources exist and are already being utilized, with geothermal energy being the focus of this work.

## 1.2 Geothermal energy and geostructure

Geothermal energy, in the thermodynamic sense, refers to the internal energy of geological materials such as rock, groundwater, and magma that constitute the Earth [6]. This energy primarily originates from the radioactive decay of elements such as uranium, thorium, and potassium within the Earth's mantle. It is transferred from regions of high internal energy to those of lower internal energy in the form of heat. Depending on the depth and temperature of the resource, geothermal energy can be classified into three categories [7]:

- Shallow geothermal energy ($<$ 400 m): It is a very low enthalpy energy source that can be harnessed. The temperature range is from 2°C to 30°C.
- Medium geothermal energy($<$ 3000 m): It is a low-enthalpy energy source that can be harnessed. The temperature range is from 50 to 100°C.

- Deep geothermal energy (>3000m): It is a high-enthalpy energy source that can be harnessed with a temperature greater than 100°C.

Figure 1.1 illustrates the different types of geothermal energy and possible applications (electricity generation and/or heat production).

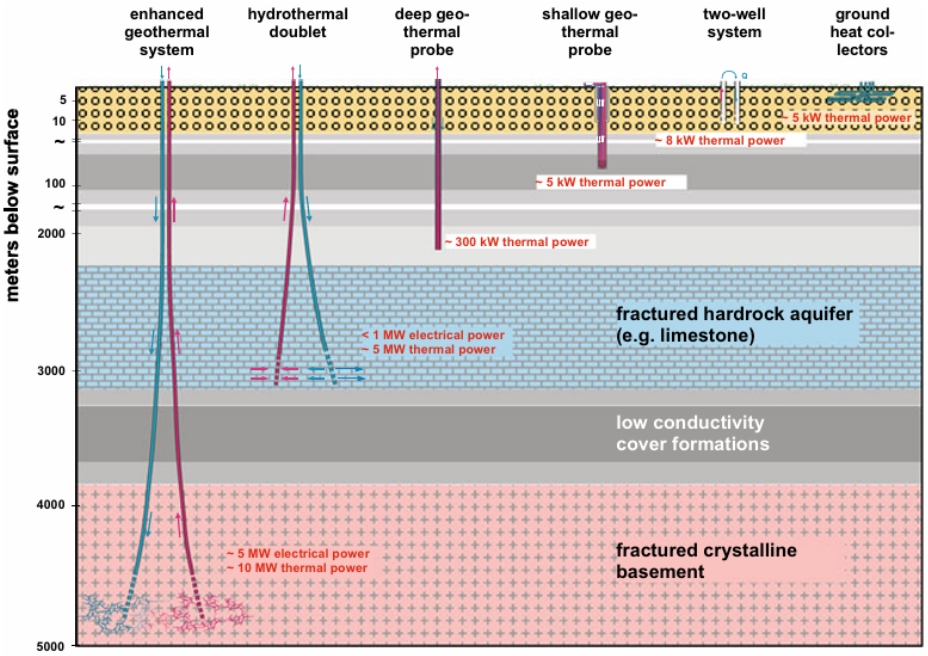


Figure 1.1: Illustration of the different types of geothermal energy based on depth in the ground.

A geostructure is a civil engineering structure designed to interact with the ground and perform a mechanical role [8]. These structures include foundations, retaining walls, piles, and tunnel linings, and they are increasingly being used for thermal purposes as well. This is due to their large contact surface with the ground, which maintains an almost constant temperature throughout the year. In addition, the spread of heat pump technologies that use ground heat as a source supports the development of energy geostructures that fall into the category of shallow geothermal energy.

## 1.3 State of the art

The socio-economic development of cities is accompanied by increased traffic on the roads and a lack of space. As a result, more and more underground structures are being built, such as underground car parks, metro tunnels, train tunnels, etc. These underground structures are not passive because they consume electrical energy to power various devices such as sensors, traffic lights, fans, etc. Given the increasing number and size of these structures, the tunnelling industry is not left out of the energy transition. For decades, studies have been conducted on the possibility of harnessing geothermal energy for urban heating, to make tunnels energy neutral, meaning that they generate the energy they consume. Studies have identified two geothermal energy harvesting systems in tunnels: closed systems and open systems.

### 1.3.1 Geothermal energy harvesting systems in tunnels

#### 1.3.1.1 Open systems or Hydro-geothermal tunnel systems

When a tunnel is excavated in a saturated area, it acts as a drain by creating a depression. The water infiltrates and stagnates at the level of the tunnel cavity [9]. It is necessary to drain it to prevent disrupting the natural flow of water underground and to preserve the tunnel's structure. The thermal energy of the warm water drained from the rock above the tunnel is used by open systems, instead of sending this water to cooling towers to lower the temperature to the discharge threshold before releasing it into watercourses [10]. Figure 1.2a shows an illustration of the open system, which includes drainage pipes to move drained water from the tunnel to the consumer, a heat pump to raise the temperature if necessary, the consumer who will extract the contained thermal energy, and a river that serves as a spillway.

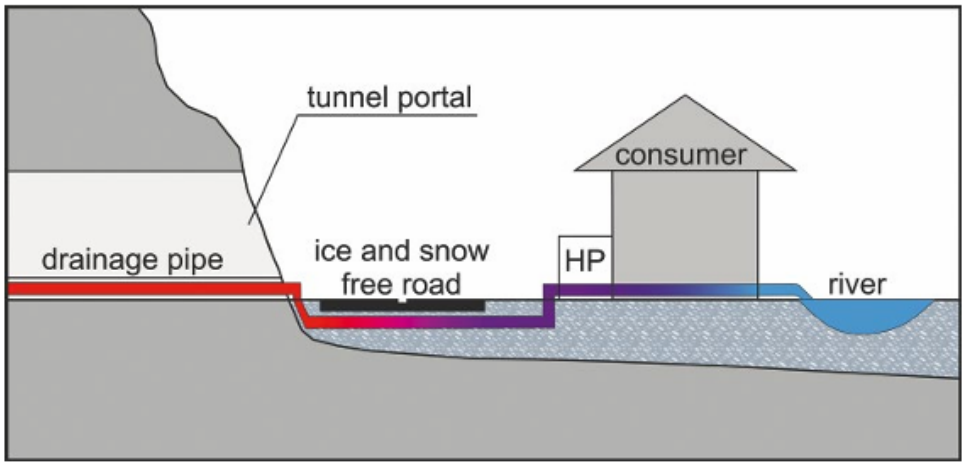


(a) Overall principle of an open system, from drainage to final use [10].

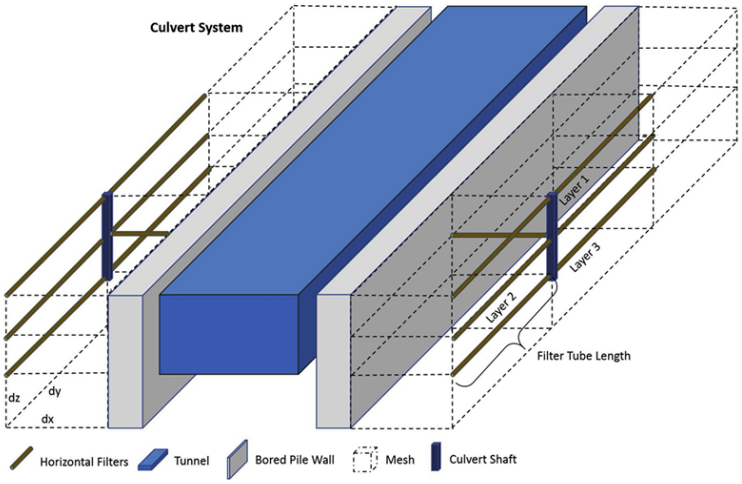


(b) Technical diagram of the drainage system [9].

Figure 1.2: Overall principle and technical diagram of the open system.

The heat flux of this system is simply calculated as follows [10]:

$$\dot{Q} = \dot{V} \rho_w c_{p,w} \Delta T$$

Where, $\dot{V}$ is the drainage water outflow rate, $c_{p,w}$ is the water specific heat capacity and $\rho_w$ the water density, $\Delta T$ is the temperature difference of the drained water between its outlet temperature and the temperature after energy extraction.

#### 1.3.1.2 Closed systems or absorber tunnel system

Tunnels have the advantage of a large contact surface with the ground and involve a significant volume of ground for heat exchange [11]. Another approach is to use the ground's temperature to heat or cool a heat transfer fluid; this approach is known as the absorber tunnel system. Figure 1.3 illustrates a closed system comprising two heat exchanger pipe loops: one on the tunnel side and the other on the end-user side [10]. Between these loops, a heat pump can be installed to increase the temperature as necessary, depending on the consumer's requirements and the ground temperature surrounding the tunnel. As illustrated in the Figure 1.3, a heat pump is a thermodynamic system consisting of two heat exchangers (called the evaporator and the condenser), a compressor, and an expansion valve. Its operating principle involves a heat transfer fluid that evaporates at low temperature by absorbing heat from a cold source at the evaporator. The fluid is then compressed by the compressor, which increases its temperature through electrical work. Finally, it releases its heat to a warmer medium in the condenser before passing through the expansion valve to restart the cycle.

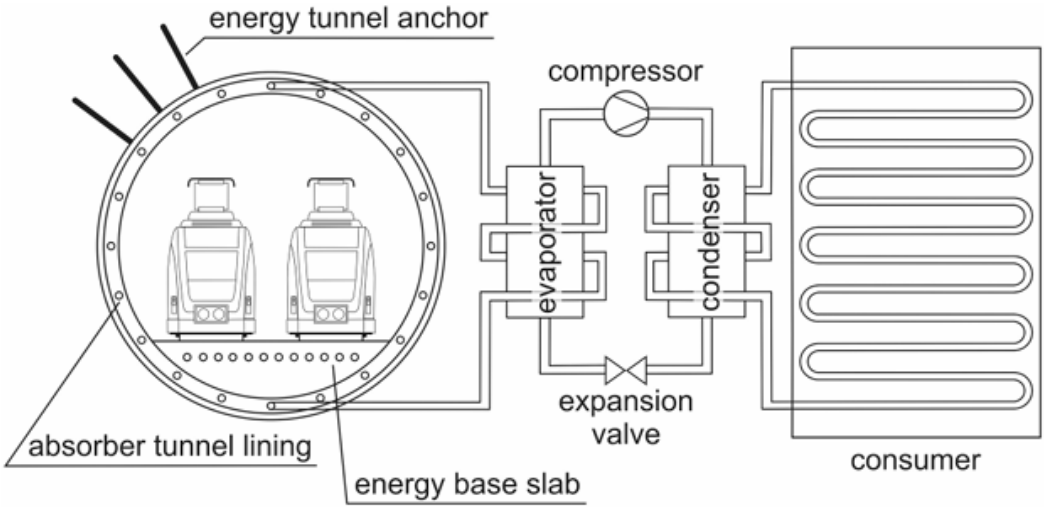


Figure 1.3: Overall principle of a closed system, with a primary loop, a secondary loop, and an intermediate heat pump.

Heat from the ground is recovered by a heat transfer fluid, which passes through heat exchange pipes integrated into the structure. In this way, the structure is thermally activated while its integrity is maintained to perform its primary function. This process is called thermal activation. Pipes are made of reticulated polyethylene (Pe-Xa) and are capable of withstanding high pressure, high temperature, and corrosion. The thermo-fluid is a mixture of propylene glycol and water that is capable of operating at temperatures as low as -20°C [11]. There are two possible ways to integrate the pipes into the tunnel structure, depending on the construction method:

- If the tunnel is excavated in a conventional manner, heat exchanger pipes are enclosed between two layers of geotextiles, forming an energy fleece. This fleece is then placed between the primary and secondary linings during the tunnel excavation. Figure 1.4 shows an example of an energy fleece.

Figure 1.4: Integration of Pe-Xa pipes into a conventionally excavated tunnel.

- If the mechanised tunnelling method is used, which involves using machines to place precast segmental linings, the heat exchanger pipes are embedded into the concrete during the manufacturing of the lining segments at the factory. Figure 1.5 shows precast lining segments (Figures 1.5b, 3.3b), and the assembly in ring into the tunnel (Figures 1.5a, 1.5d) [12].

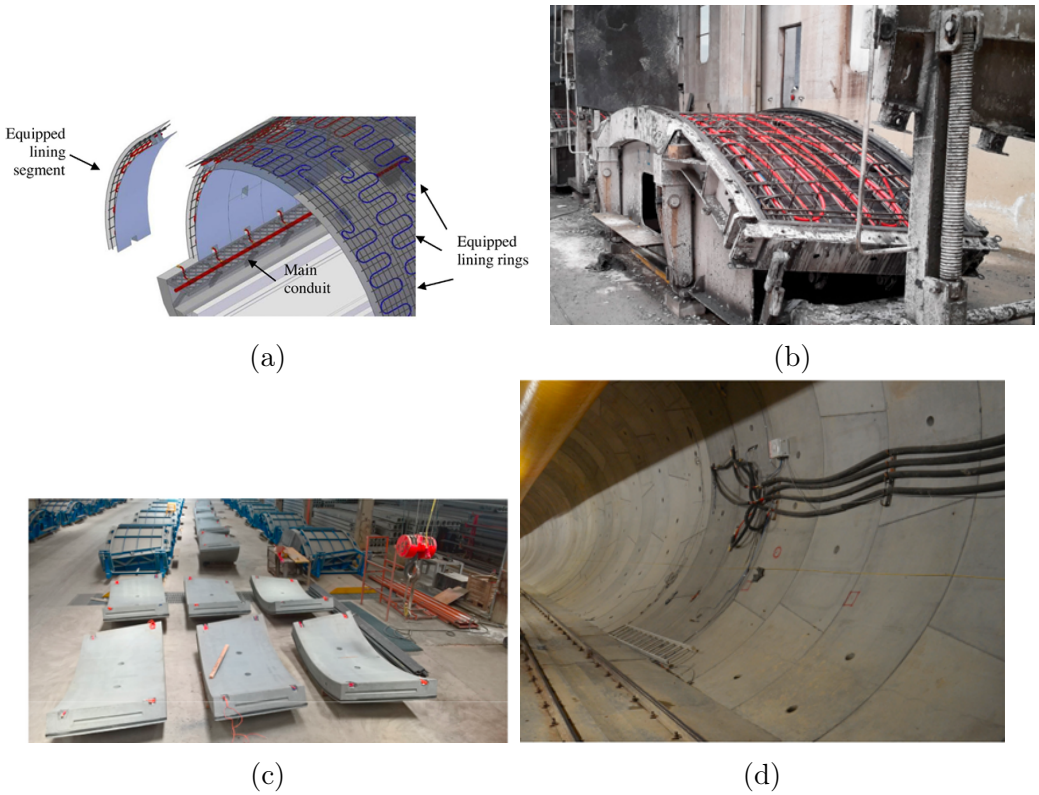


Figure 1.5: Prefabricated tunnel lining segments with integrated Pe-Xa pipes, lining ring Assembly Inside the Tunnel.

Additionally, depending on whether heat exchange occurs with the surrounding rock, with the air inside the tunnel, or with both, the pipes are positioned either near the interior of the tunnel or close to the ground, as shown in the Figure 1.6 [12].

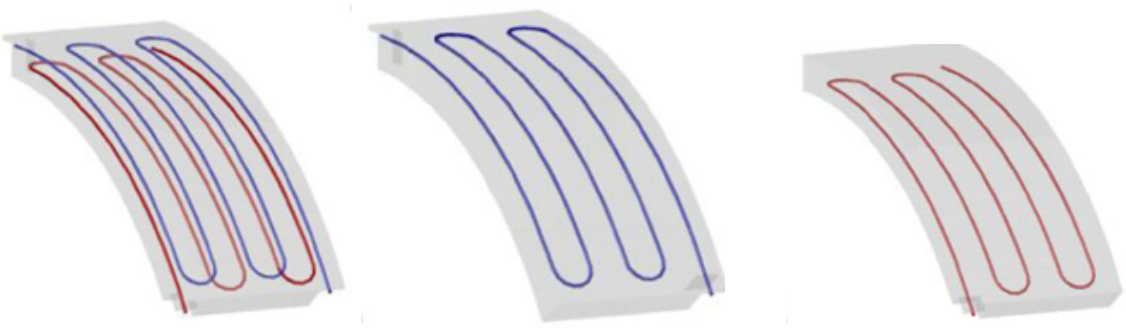

(a) Ground and air-side pipe. (b) Ground-side pipe. (c) Air-side pipe.

Figure 1.6: Different positions of heat exchanger pipes.

### 1.3.2 Some Pilot Projects

In Europe, several feasibility studies have been carried out on geothermal energy through tunnel activation in various tunnels. Some of these studies have led to pilot projects and even to the implementation of complete systems. Two representative examples are the pilot project on Line 1 of the Turin metro in Italy and the Lötschberg Base tunnel in Switzerland. A common feature among these pilot projects is that the entire length of the tunnel is not thermally activated. Instead, preliminary thermo-mechanical studies are conducted to identify zones with the highest potential.

#### 1.3.2.1 Turin Metro, Line 1, Italy

Turin Metro Line 1 was inaugurated in 2006. In 2021, a new southern extension was under construction, spanning 1.9 km with a diameter of 8 m. This extension, linking Lingotto to Piazza Bengasi, was commissioned on April 23, 2021. The tunnel was excavated to a depth of 21.5 m, positioned below the groundwater table. The tunnel lining consists of precast concrete rings, each 30 cm thick. Each ring is composed of seven segments, assembled in situ using a tunnel boring machine. The geological profile of the Turin underground includes sand, gravel deposits, and cemented soil below 10 m, with the water table at a depth of 12 m. The aquifer spans 23 m in width and maintains an average water temperature of 14°C [13].
As a prototype, two fully thermally activated rings, incorporating a double ground-air configuration, were installed approximately 42 m before the station entrance, with a total length of 2.80 m [14]. Numerical and experimental investigations indicate that, based on collected data, the extractable thermal power during winter ranges between 42 and 52.5 $W/m^2$, while in summer, the injectable power varies between 60.5 and 66.4 $W/m^2$ [12].

#### 1.3.2.2 Lötschberg base tunnel, Switzerland

The Lötschberg Base Tunnel, operational since 2007, is a 34.6 km railway tunnel connecting the Bernese Oberland to the canton of Valais. It traverses the Swiss Alps, passing through a complex geological mix of sandstones, schists, carbonates, and crystalline rocks, with a maximum rock overburden of approximately 2 km. The tunnel drains water at a rate of about 100 litres per second, maintaining a constant temperature of around 20°C. The drained water is used in a cascading system: initially, it supplies a fish farm in Frutigen, producing approximately 45 t of thermophilic Siberian sturgeon, 20 t of perch, and 2 to 3 tof sturgeon caviar annually [10]. Subsequently, additional heat is extracted via a

heat pump to support a greenhouse. Before being discharged into local water bodies, the remaining thermal energy is harnessed through a district heating network in Frutigen.

## 1.4 Contribution

Countries such as Germany, Switzerland, France, and Italy have already taken steps toward the thermal activation of tunnels, carrying out feasibility studies on various sites and even launching pilot projects. This work highlights the geothermal potential of deep railway tunnels in Belgium. Although the exact number of such tunnels is unknown, three stand out for their length and depth: the Liefkenshoek, Soumagne, and Diabolo tunnels. This study focuses on the Liefkenshoek tunnel and aims to develop a simple analytical model to represent heat exchange between the ground, the tunnel lining, and the air inside, using basic, macroscopic, measurable parameters and a straightforward approach to describe this exchange.

## 1.5 Objective and Structure of the Work

The main objective of this work is to assess the exploitable geothermal potential through the thermal activation of the Liefkenshoek tunnel. Internal documents from TUC RAIL provide information on the tunnel's geometry and the lithology identified during geotechnical investigations before construction. However, these sources reveal a significant limitation: the lack of detailed thermal soil properties such as conductivity, heat capacity, and the undisturbed ground temperature profile. These properties are essential, as they directly determine the amount of heat that can be extracted and thus strongly influence the accuracy of any feasibility assessment. This leads to the following questions: What type of geothermal system does the Liefkenshoek tunnel correspond to? How can the necessary thermal properties be measured? How does heat transfer occur, and how can it be modelled? Finally, how can variations in certain parameters of the developed model impact the performance of the heat exchanger?
To address these issues, the work is organised into six chapters as outlined below:

- Chapter 2, which focuses on the tunnel case study, provides information about the geological layers crossed by the tunnel, its energy consumption, and the interior air temperature profile. Moreover, the information regarding the tunnel's construction method, executed using a tunnel boring machine (TBM) and prefabricated concrete lining, allows the conclusion that the geothermal system corresponds to a closed-loop system, as described in section 1.3.1.2.

- Chapter 3 presents a preliminary evaluation of the geothermal potential of the soil using transient analytical solutions derived from the book Fundamentals of Heat Transfer. To this end, a definition of the potential application of the geothermal resource, namely district heating, is first established. Then, the modes of heat transfer are described, and the methods for measuring the required thermal properties are explained. This chapter demonstrates that these solutions can be used to identify soils with the highest potential. However, for increased accuracy, it will be necessary to model the heat exchanger by accounting for the various thermal resistances and other existing influences.

- Chapter 4 models the heat exchanger using analytical heat transfer equations under steady-state conditions, accounting for the soil temperature, the tunnel's internal

air temperature, and the various thermal resistances to heat transfer. This chapter concludes with the validation of the analytical model developed, and also analyzes the influence of the heat transfer fluid's flow rate, the tunnel air temperature, and the inlet temperature of the heat transfer fluid on the performance of the heat exchanger.

- Chapter 5 presents a concise economic assessment of the profitability and sustainability of the tunnel's thermal activation. To this end, a simplified evaluation of the required capital expenditure and the fixed and variable operating costs is performed; the total system cost and the cost of heat produced by the system are then estimated. The chapter concludes that the decisive factor is the amount of heat exchanged by the heat exchanger; accordingly, lower inlet temperatures are preferred

- Chapter 6 presents an experimental protocol comprising the steps to be followed and their descriptions, in order to transition from the feasibility study conducted to a pilot project. This chapter also outlines future directions for extending the work carried out here.

- Chapter 7 constitutes the overall conclusion of the study.

# Chapter 2

# Liefkenshoek tunnel

## 2.1 Description of the Tunnel

The Liefkenshoek rail tunnel was built between 2010 and 2014. It aims to connect the railway freight transport between the left and right banks of the Scheldt River in the port of Antwerp. The tunnel length is around 16.2 km, and the largest part of the tunnel, which measures around 6 km, as shown in Figure 2.1, consists of twin bored tunnels excavated below the Scheldt River and the Port Canal. The twin tunnels are parallel, each with a single track, an internal diameter of 7.3 m and an outer diameter of 8.10 m. The lining is made of precast concrete elements, with a thickness of 0.4 m in C50/60 concrete quality. Each tunnel ring contains 7 segments and is 1.8 m wide [15]. The information concerning the tunnel excavation method, executed using a tunnel boring machine (TBM) and precast concrete lining, permits the conclusion that the applicable geothermal system corresponds to a closed-loop system. Indeed, the exchanger pipes are embedded within the concrete segments during their prefabrication.

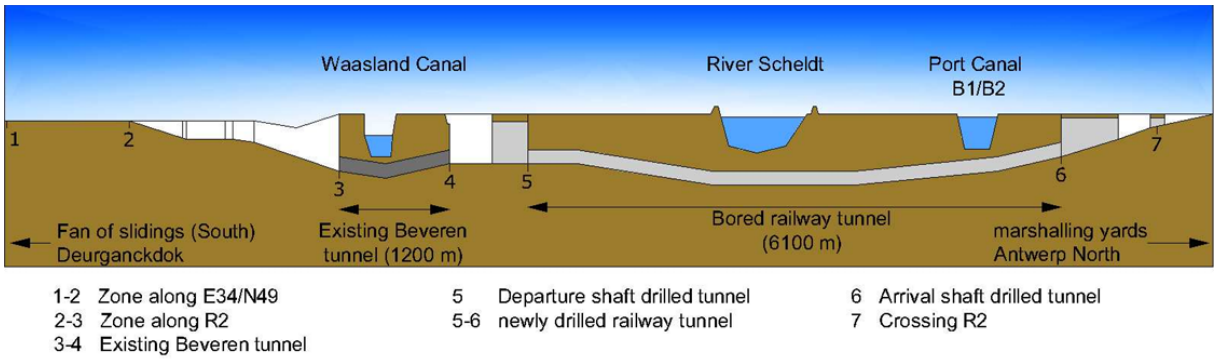


Figure 2.1: Longitudinal profile of the Liefkenshoek tunnel.

Figure 2.2 shows the geographical location of the entire Liefkenshoek tunnel and the surrounding areas.

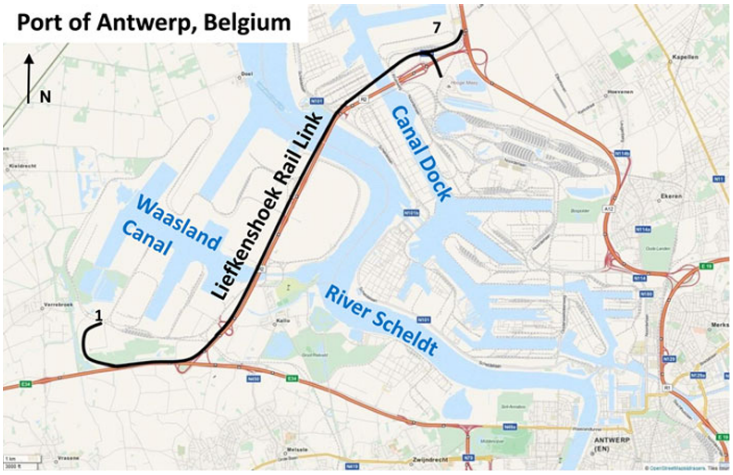


Figure 2.2: Map showing the geographical location of the Liefkenshoek tunnel.

It should be noted that this study focuses exclusively on section 5-6, which corresponds to the most recently constructed segment using the mechanised tunnelling method. It is also the deepest section, exceeding 20 meters in depth, where the surrounding temperature may reach at least 10°C.

## 2.2 Lithology of the site

The Liefkenshoek tunnel crosses different geological layers depending on the depth at which it is excavated. Figure 2.3 shows the layers crossed by sections 5-6 of the tunnel [16].

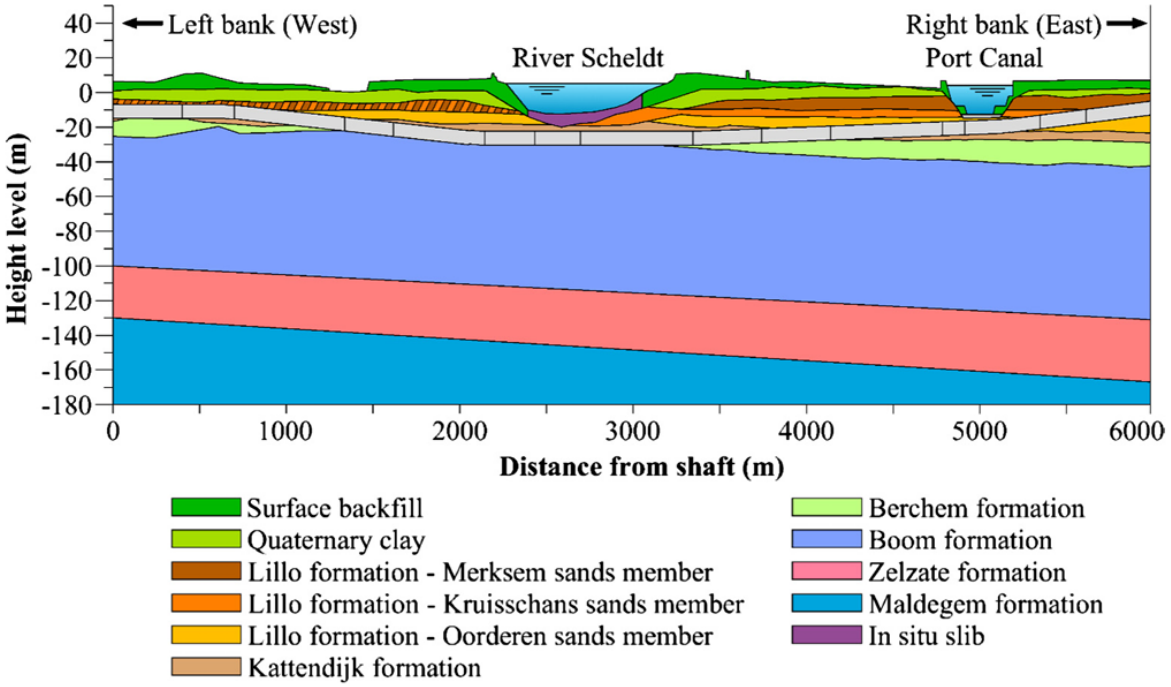


Figure 2.3: Diagram of the geological layers crossed by the tunnel.

The layers through which it passes are geological formations with different characteristics and mineralogical compositions. The main geological formations around the tunnel and

their description, according to the Belgian National Commission for Stratigraphy [17], are as follows:

- **Boom formation**: It is a grey silty clay or clayey silt, with relatively constant chemical and mineralogical properties. It contains glauconite granules and also shows pyrite formed at scales from millimetres to centimetres, even decimetres, due to the organic matter present in the clay. The thickness of this formation is around 80 m in the Antwerp region.

- **Berchem formation**: It is a unit of green to blackish sand, with fine to medium grains, sometimes very rich in glauconite and containing a small amount of clay. The average grain size ranges between 130 µm and 330 µm, and at its base is a gravel bed made of dark, rounded flint pebbles. The thickness of this formation is around 30 m in the Antwerp region.

- **Kattendijk formation**: It consists of fine to medium-fine sand, dark grey to grey-green in colour, rich in glauconite (around 20%), mainly made up of quartz with a slight clay content. The maximum thickness of this formation is about 15 m in the Antwerp region, and a basal gravel layer is found, made of rounded pebbles of quartz and flint, along with shark teeth, sandstone, phosphatic nodules, and rounded bones.

- **Lillo formation**: It consists of shelly sand with a clayey mix in the central part, and several distinct shell layers. The colour ranges from grey, grey-brown to light brown-grey. The glauconite content is relatively constant, varying between 6 and 12%. The formation is subdivided into several members, including the Oorderen Member, Kruisschans Member, and Merksem Member. The maximum thickness of this layer is 30 m.

So, based on the different descriptions of the geological formations, the tunnel passes through sand with varying grain sizes and colours, as well as clay, all rich in glauconite. The cross sections obtained from internal TUC RAIL files confirm that the tunnel primarily passes through sandy layers, with some occurrences of clay as well, as shown in Figure 2.4.

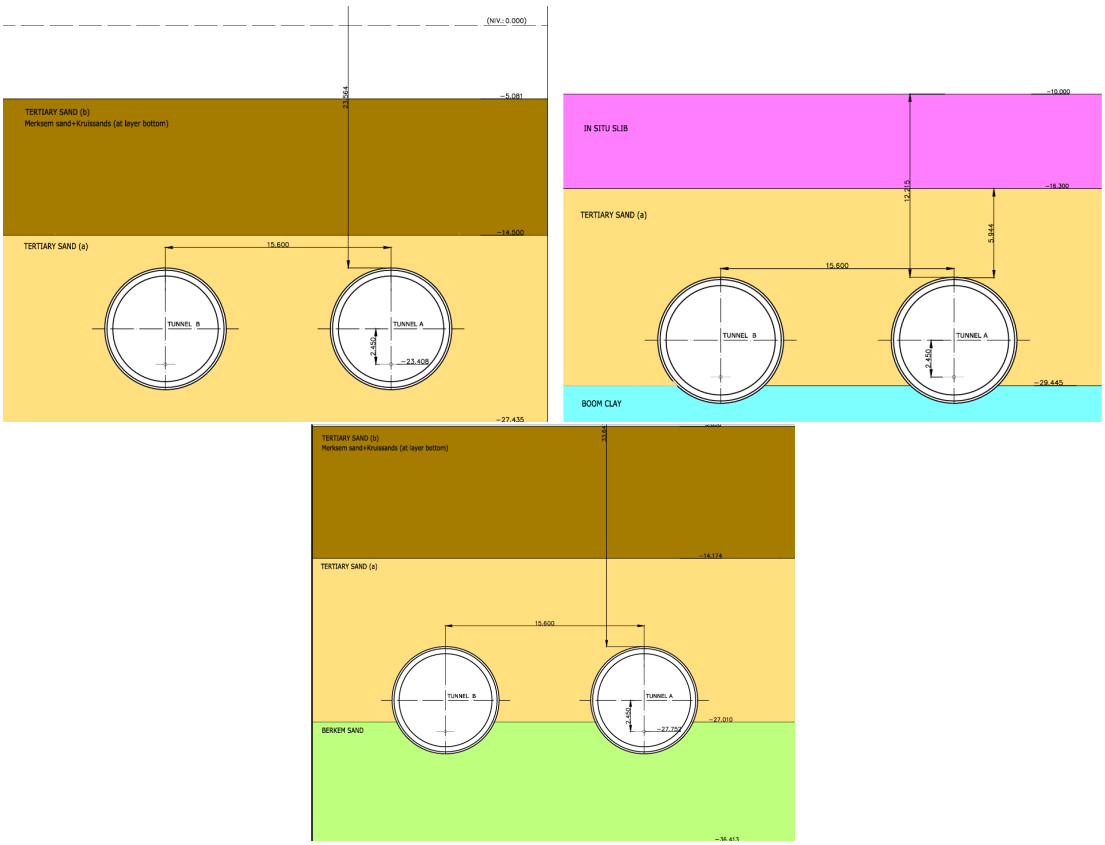


Figure 2.4: Cross-sectional view of the tunnel.

Table 2.1 provides a summary of the properties of sand and clay, depending on whether they are dry or water saturated [18].

| **Rock type** | **Thermal conductivity** $k$ [W/(m·K)] | | **Volumetric heat capacity** $\rho c_p$ [MJ/(m³·K)] | **Density** $\rho$ [$\times 10^3$ kg/m³] |
|---|---|---|---|---|
| | Effective value | Recommended value | | |
| Clay/silt, dry | 0.40 – 1.00 | 0.50 | 1.5 – 1.6 | 1.80 – 2.00 |
| Clay/silt, water-saturated | 1.10 – 3.10 | 1.80 | 2.00 – 2.80 | 2.00 – 2.20 |
| Sand, dry | 0.30 – 0.90 | 0.40 | 1.30 – 1.60 | 1.80 – 2.20 |
| Sand, moist | 1.10 – 1.90 | 1.40 | 1.60 – 2.40 | 1.90 – 2.30 |
| Sand, water-saturated | 2.00 – 3.00 | 2.40 | 2.20 – 2.80 | 1.90 – 2.30 |
| Silica/rock, dry | 0.40 – 0.90 | 0.60 | 1.60 – 2.00 | 1.90 – 2.20 |
| Silica/rock, water-saturated | 1.60 – 2.50 | 1.80 | 2.20 – 2.60 | 2.10 – 2.40 |
| Clayey clay/clay | 1.10 – 2.90 | 2.40 | 1.50 – 2.50 | 1.80 – 2.30 |

Table 2.1: Summary of the properties of the identified geological layers.

## 2.3 Temperature profile

The tunnel is equipped with sensors that measure air temperature and humidity inside. This temperature can be representative of the ground temperature, due to heat exchange between the soil and the tunnel air through the concrete. Moreover, the air temperature inside the tunnel is also influenced by several external factors: the ambient outside air temperature entering the tunnel, the ventilation system, and the heat generated by train traffic; as illustrated in Figure 2.5.

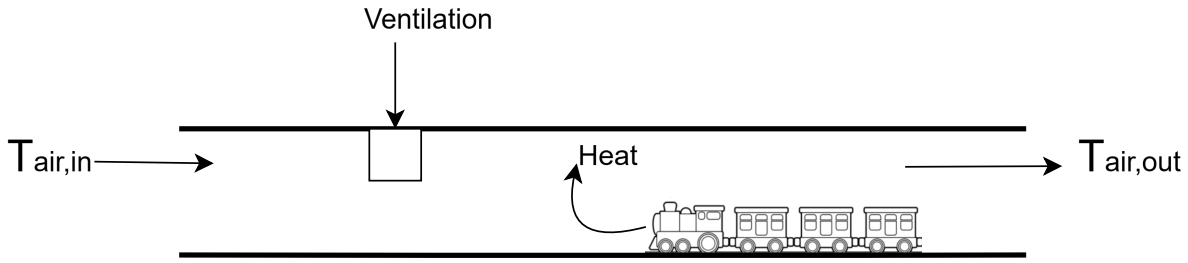


Figure 2.5: Establishment of the air temperature in a tunnel.

The collected data provided by the maintenance team covers the period from August 2014 to March 2015.

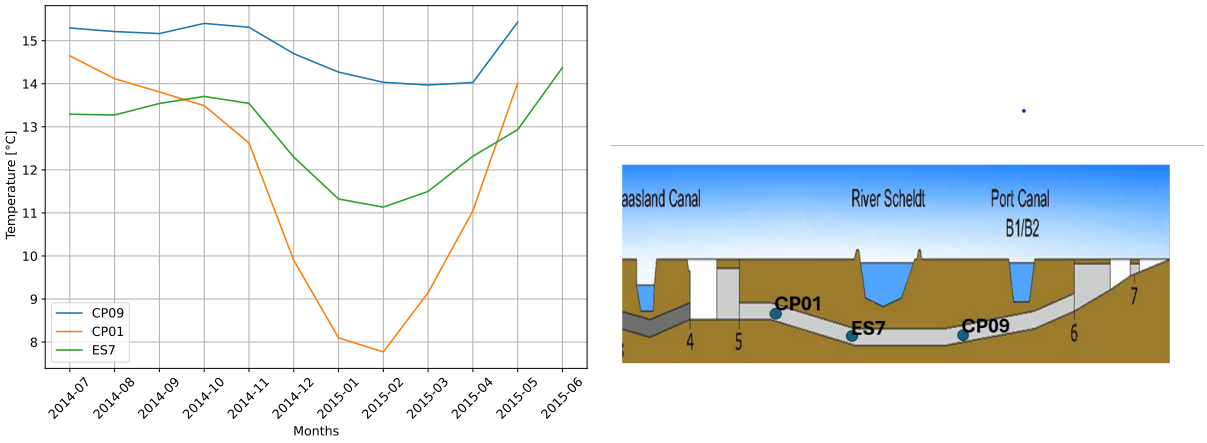


(a) Monthly average temperature. (b) Temperature measurement zone.

Figure 2.6: Monthly average temperature measured in three zones of the tunnel.

Figure 2.6 shows the monthly average temperature for three zones within the tunnel. The observed trend, as expected, shows higher temperatures during the summer months and lower temperatures during the winter months. The range of interior air temperature during the winter is between 8 and 14°C. For the remainder of this study, a uniform temperature of 11°C (median value of the interval) along the entire length of the tunnel is assumed.

## 2.4 Electrical Energy Consumption of the Tunnel

As mentioned, tunnels are not passive structures; they consume electricity to operate their equipment. Fixed equipment in tunnels in general and in railway tunnels in particular, includes:

- Signalling lights,
- Railway system management equipment,
- Data transmission networks,
- Telecommunication devices such as radios, loudspeakers, and telephone networks,
- Lighting,
- Ventilation,

- Drainage systems,
- Fire detection and emergency response systems.

Data on the electrical consumption in MWh for the tunnel studied in 2022 show an annual usage of 516.981 MWh. Figure 2.7b illustrates the monthly consumption profile, which reveals significant variation throughout the year. However, this consumption tends to be higher during winter and spring (from November to May). Additionally, the electrical consumption of the tunnel fluctuates hourly throughout the year, as illustrated in Figure 2.7a, with noticeable peaks at specific times. The discussion with the maintenance team explains these peaks, which are due to the use of dehumidifiers that activate when humidity levels are high, as well as the ventilation system, which turns on 10 to 12 times per day when CO levels are elevated.

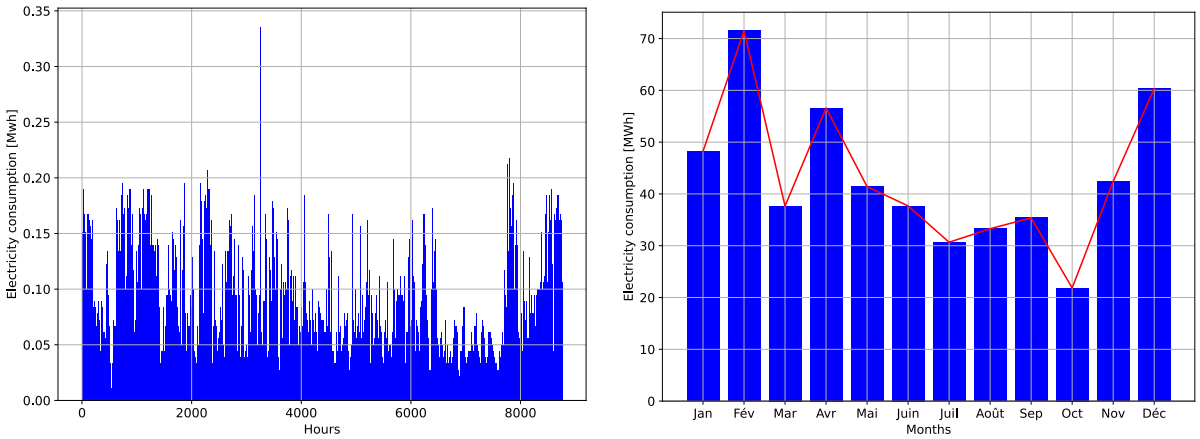


(a) Electrical energy consumption per hour. (b) Electrical energy consumption per month.

Figure 2.7: Electrical energy consumption per hour and month of the tunnel in 2022.

In summary, Chapter 2 provides an overview of the Liefkenshoek tunnel, covering its geographical context through to its annual electricity consumption in 2022. This chapter enables a clear identification of the geological layers crossed by the tunnel, the geometry of the tunnel and the internal air temperature, providing precise and essential data for evaluating the geothermal potential in the subsequent chapters.

# Chapter 3

# Transient evaluation of geothermal potential

The Liefkenshoek tunnel has been studied in the previous section, from its geometry to its annual electrical consumption, including the lithostratigraphy of the site where it is located. The focus now is to evaluate the exploitable geothermal potential along the tunnel. To this end, the possible use of this potential is first defined based on the classification of geothermal systems. This is followed by an assessment of the potential using analytical heat transfer solutions, assuming a homogeneous medium in terms of both thermal properties and temperature. This chapter employs transient analytical heat transfer solutions derived from *Fundamentals of Heat and Mass Transfer* [19]. These solutions consider only the soil properties and the initial temperature gradient (the undisturbed ground temperature and the tunnel surface temperature). The aim here is to determine whether these solutions are sufficient to estimate the geothermal potential of a thermally activated tunnel. The evaluation of geothermal potential in a transient framework also helps to observe how it evolves.

## 3.1 Application description

Geostructures in general, and tunnels in particular, fall into the category of low-enthalpy geothermal systems due to their depth being less than 400 m . In addition, in Europe, the geothermal gradient in areas outside volcanic regions is approximately 3°C per 100 m. The ground temperature remains constant, ranging between 10 and 12°C, beyond a depth of 10 m, as shown in Figure 3.1, coming from Scientific and technical centre for the construction [18]. The deepest section of the Liefkenshoek Tunnel (section $5-6$) lies between 20 and 40 m below ground, and the measurements of the internal air temperature within the tunnel support the strong assumption that the ground temperature ranges between 10 and 12°C.

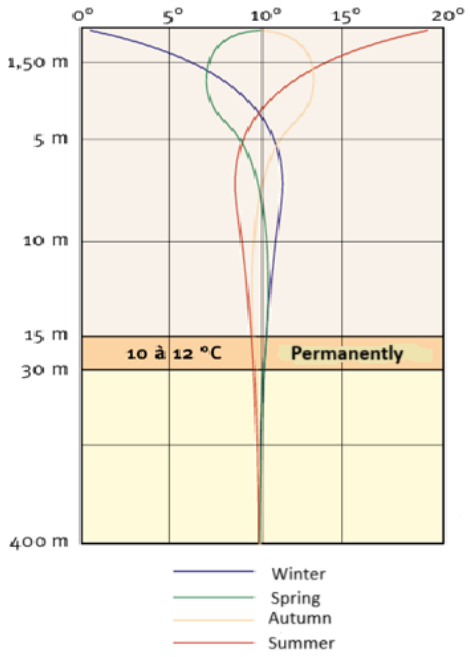


Figure 3.1: Ground temperature profile with depth.

Thus, in the best-case scenario, the outlet temperature of the heat transfer fluid is, at most, 12°C. As a result, a heat pump is required to raise the fluid's temperature before it can be used. As mentioned earlier, a heat pump is a thermodynamic device that extracts heat from a cold source and transfers it to a warmer one, using electrical work to increase the temperature. The higher the outlet temperature of the heat pump, the greater the electrical work required. Consequently, district heating emerges as the most viable application, with operating temperatures ranging from 30 to 35°C for networks employing floor or wall heating systems and from 50 to 60°C for those using radiators as heat emitters. In contrast, electricity generation using currently available technologies requires high temperature levels. However, the temperatures observed in this case are very low, and using a heat pump or any other thermodynamic system to reach the necessary levels would require a significant amount of energy, thereby greatly reducing the overall efficiency of the system. As a result, electricity generation is not a viable option in this context.

A district heating network is a system that generates and distributes heat on a large or small scale. It includes one or more thermal energy sources, a distribution network, and substations. Regarding heat sources, production can be carried out at a single location, known as centralised production. However, there can also be decentralised production units that convert primary energy into distributable energy. Figure 3.2 illustrates two examples of heating networks using geothermal energy as a heat source [20]. The first features a large central heat pump that raises the temperature to the distribution level. The second involves small heat pumps at each end user's site, meaning that the network temperature corresponds to the outlet temperature of the geothermal heat exchanger.


Figure 3.2: District heating network with geothermal heat pump.

In the following analysis, centralised district heating at 35°C, using floor heating systems as emitters, is considered as the target application. It is assumed that the full exploitable thermal potential is available for use. The analysis focuses solely on the geothermal heat exchangers and the heat pump. With the application clearly defined, the exploitable potential can now be determined.

## 3.2 Transient state analytical solution

The analysis of transient heat transfer makes it possible to compare different heat transfer configurations, as well as various soil types. In this study, the heat exchange configuration remains unchanged; only the thermal properties of the soil vary. This analysis aims to determine, for each ground type, how the thermal potential evolves until reaching a steady state during heat extraction, and to identify which soil offers the best thermal potential at steady state. Thus, the first step is to identify the heat transfer modes that take place, followed by the use of analytical solutions to evaluate the thermal potential, and finally, to discuss the results.

### 3.2.1 Heat transfer mode into the ground.

Heat transfer in the soil occurs through two main modes, namely:

- **Conduction**
  It is the transfer of heat within a medium under a temperature gradient. It is described by Fourier's law $q = -k\nabla T$, where k is the thermal conductivity of the medium. In the case of geothermal energy, the heat transfer medium is the ground, which is a mixture of rock, water, and air. The thermal conductivity measures the ability of that mixture to conduct heat. Another property that influences this mode of transfer is the specific heat capacity of the rock and the density, which defines the material's ability to store heat. These properties can be determined:

  – The thermal conductivity (k) can be determined theoretically or in the laboratory, based on the rock's composition, void ratio, permeability, and by applying the weighted average of k of the individual components of the soil. Experimentally, on-site, it is determined through a Thermal Response Test (TRT), which uses the transient line source method [7]. The test involves injecting a controlled heat flux into a geothermal borehole through borehole heat exchangers, then measuring the thermal response of the ground over time and space. The slower the temperature of the ground increases, the higher the thermal conductivity. There are also portable commercial devices, such as the Portable

Electronic Divided Bar (PEDB), which can measure not only thermal conductivity but also specific heat capacity of a soil sample.

- The specific heat capacity(c) is measured in the laboratory on a sample using a calorimeter, and the density ($\rho$)is determined based on Archimedes' principle.
- Ground temperature($T_{ground}$) Influences heat conduction due to the existing thermal gradient. To determine ground temperature, data from previously drilled boreholes in the region can serve as a reference for new projects [7]. Experimentally, temperature sensors are used to measure ground temperature at various depths as the borehole is being drilled. These data are then interpolated and extrapolated to estimate the temperature at different depths within the ground.

- **Advection**
  Heat transfer by advection is related to the movement of fluid within the soil, which results in a continuous recharge of heat in the ground. This mode is linked to the flow velocity of the fluid, most often the water contained in the soil, and is expressed as $\rho_w c_w \nabla(Tq)$, with $\rho_w$ water density, $c_w$ water heat capacity, and q Darcy groundwater velocity [21]. This velocity can be computed as the product of porosity and the groundwater flow velocity, or measured using methods such as tracer tests and with instruments like flow meters, current meters, and piezometers equipped with pressure sensors, all of which are commercially available.
  Figure 3.3 shows some examples of devices or measurement principles used to assess the thermal properties of the soil, as mentioned above.

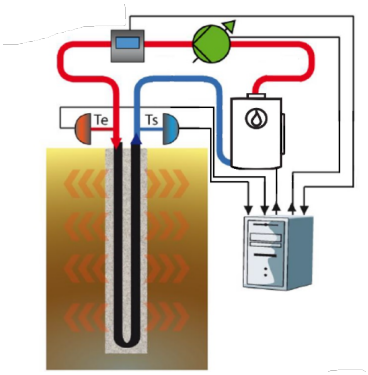


(a) Example of Thermal Response Test(TRT) principle [22].

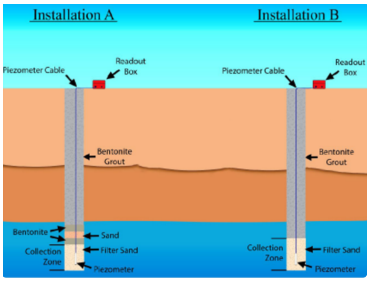


(b) Example of piezometer installation [23].

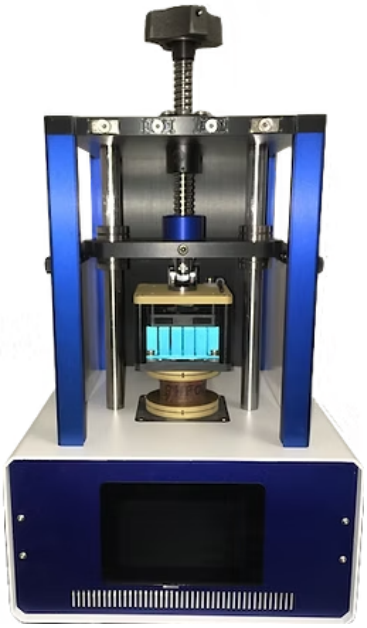

(c) Example of Portable Electronic Divided Bar (PEDB) [24].

Figure 3.3: Some examples of instruments and measurement principles for determining soil properties.

Now that the modes of heat transfer in the soil and the relevant soil properties are known, the analytical solutions governing heat transfer can be applied. It is important to note

that, for now, the flow velocity in the soil will be considered zero, and the effect of this parameter will be analysed at a later stage.

### 3.2.2 Equations

The first step is to determine the dimensionless amount of heat that can be extracted from the ground, which is then scaled to real-world units. This dimensionless heat depends solely on the properties of the soil, the heat transfer configuration, and the mode of heat transfer. The configuration considered involves two-dimensional conduction, where the ground is treated as an infinite, homogeneous medium, both in terms of its thermal properties and initial temperature. The tunnel is modelled as a cylinder with a constant surface temperature embedded within this medium. The formula is as follows [19]:

$$q^* = \frac{1}{\sqrt{\pi Fo}} + q^*_{ss} \tag{3.1}$$

$$Fo = \frac{\alpha t}{L_c^2} \tag{3.2}$$

$$\alpha = \frac{k}{\rho c} \tag{3.3}$$

$$L_c = \left(\frac{A_s}{4\pi}\right)^{(1/2)} \tag{3.4}$$

$$A_s = \pi D_{out} L_r \tag{3.5}$$

with

- $q^*$: the dimensionless amount of heat,
- Fo: the Fourier number,
- t: the time interval over which the transient state is analysed, it is set to 3 years,
- $L_c$: the characteristic length,
- k: the ground's thermal conductivity, equal to 2.40 W/mK for water saturated sand, 1.40 W/mK for wet sand, and 1.80 W/mK water saturated clay (Table 2.1),
- $\alpha$: thermal diffusivity coefficient of the ground,
- c: the specific heat capacity of the ground,
- $\rho$: density (Table 2.1),
- $A_s$: the active area, the lateral surface of the cylinder in this case,
- $q^*_{ss}$: the steady-state analytical solution for heat transfer between an infinite medium at a given temperature and a cylinder of defined length and diameter at a different temperature. The calculation of this parameter is done by knowing the heat transfer configuration, using shape factor S in m to calculate the heat transfer rate in watts (Q) and then converting this value into its dimensionless form. The formulas used are:

$$Q = Sk\Delta T \tag{3.6}$$

$$q^*_{ss} = \frac{QL_c}{kA_s\Delta T} = \frac{SL_c}{A_s} \tag{3.7}$$

The shape factor used in this context is taken from the *VDI Atlas Heat book* and will be detailed in the Results section.

### 3.2.3 Results

Figure 3.4 from the *VDI Atlas Heat book* shows the heat transfer configuration and the shape factor $S_r = \frac{S}{r}$ associated with different ratios between the radius (r) and the mid-length.

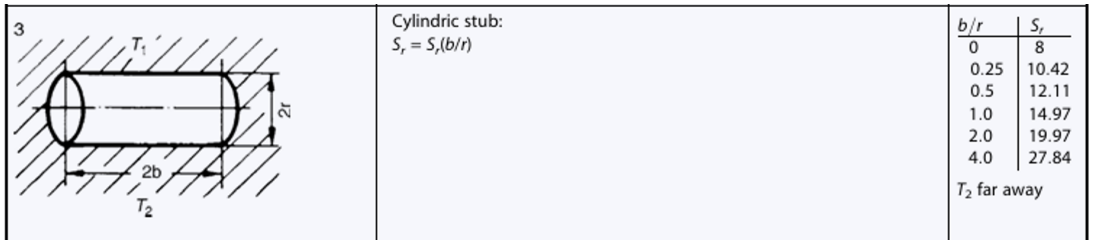


Figure 3.4: Heat transfer configuration.

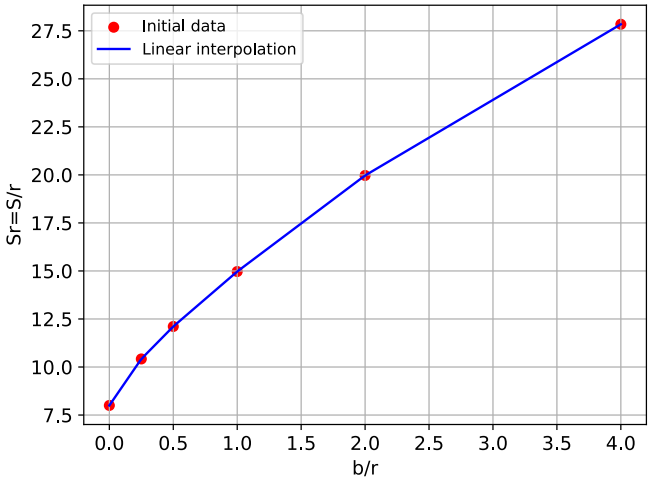


Figure 3.5: Shape factor interpolation.

By linear interpolation of the existing points, the curve in figure 3.5 shows an almost cubic trend in the shape factor $S_r$ with respect to the ratio $b/r$.
Now that the method for selecting the shape factor is known, the dimensions of the cylinder must be set or imposed. For the radius, the outer radius of the tunnel is used $2r = 8.10\,\text{m}$. For the length, in line with the ENERTUN profile by Marco Barla [12] — which involves activating segments and connecting them in series to form a lining ring (ring-by-ring activation), and then connecting different rings along the tunnel's length in parallel— the length is therefore $2b = 1.8\,\text{m}$
Section 2.2 identified sand and clay as the main materials encountered along the tunnel path, and their physical properties were listed based on values from the literature. Moreover, internal documents from TUC RAIL on tensile tests performed on samples taken from the study site show a water content ranging from 85% to 95%. Therefore, the assumption of water saturated sand and water saturated clay medium is justified. Assessing the exploitable geothermal potential is possible using the thermal properties of these soils. The potential will therefore be evaluated by focusing on a lining ring, and Table 3.1 provides a summary of the tunnel dimensions and lining ring.

| Dimensions | Symbol | Value | Unit |
|---|---|---|---|
| Inner tunnel diameter | $D_{in}$ | 7.30 | m |
| 0uter tunnel diameter | $D_{out}$ | 8.10 | m |
| Lining thickness | $e$ | 0.4 | m |
| Lining ring axial length | $L_r$ | 1.8 | m |

Table 3.1: Summary of tunnel ring dimensions.

Figure 3.6a shows the evolution of the dimensionless heat potential for soils composed of saturated sand, or wet sand, and or saturated clay, as a function of the Fourier number. The three soil types show a similar evolution as the curves overlap, which is the expected result since the heat transfer configuration remains unchanged. The only difference lies in the value associated with the Fourier number after 3 years. The Fourier number represents dimensionless time. A larger Fo indicates that the transient has decayed further and the system is closer to the steady state. Consequently, at a fixed time, the material with higher thermal diffusivity (water saturated sand) reaches steady state conditions more quickly than saturated clay or wet sand.

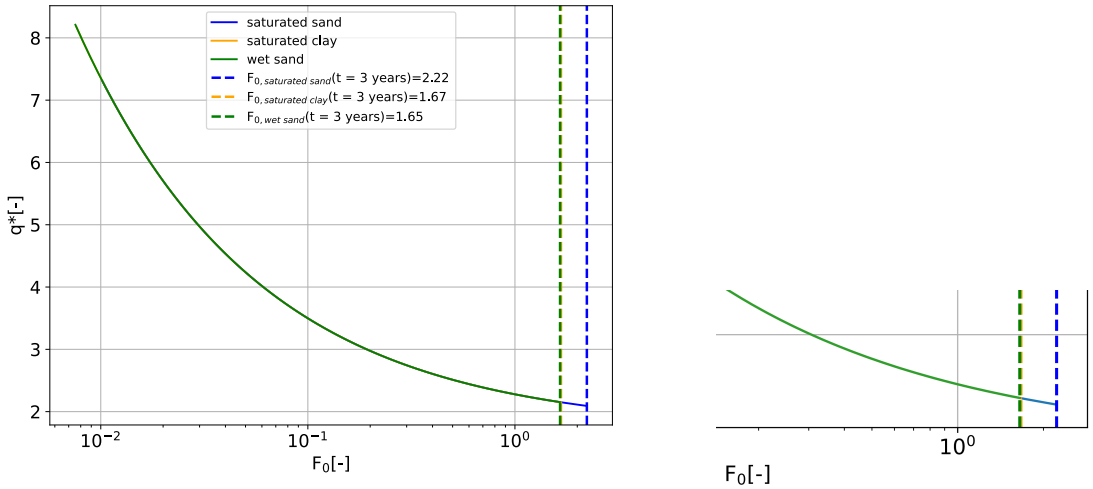


(a) (b)

Figure 3.6: Evolution of the dimensionless heat over 3 years of heat extraction.

### 3.2.4 Geothermal potential per surface unit

The dimensionless potential $q^*$ does not account for ground temperature. To include this parameter, the heat quantity must be converted back into physical units. This requires knowledge of the ground temperature at the depth where the tunnel is excavated. In the previous section, the assumption of a ground temperature equal to 12°C was validated. Furthermore, a constant temperature $T_s$ must be imposed over the entire cylinder surface. A value of 4°C is imposed, as it is widely referenced in the literature as the typical inlet temperature for the heat transfer fluid. Equation 3.8 is used for resizing. The heat quantity is expressed in W/m$^2$, and it also shows the direct impact of the ground's thermal conductivity on the amount of exploitable heat, for a given temperature difference.

$$Q_{\text{transient}} = \frac{k(T_{ground} - T_s)q^*}{L_c} \tag{3.8}$$

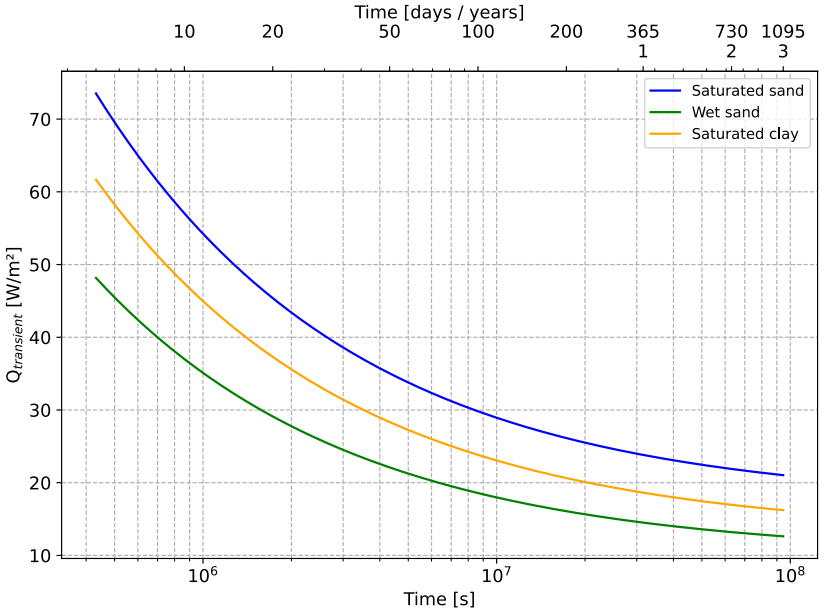


Figure 3.7: Evolution of transient heat potential.

Figure 3.7 shows how the heat flux from the ground to a cylindrical surface at constant temperature evolves. It illustrates that higher soil thermal conductivity corresponds to greater exploitable potential. The curves also exhibit a rapid decline at the onset of extraction, which progressively diminishes over time and approaches a steady-state condition. This indicates that the transient state evolves into the steady-state solution. To conclude, after three years of operation, a sandy soil will have a geothermal potential of about 21 $W/m^2$, while a clayey soil will reach around 15 $W/m^2$. All of this confirms that water saturated sand exhibits superior heat extraction performance over time, despite its relatively rapid thermal discharge and quick approach toward steady state.
Up to this point, only the soil's response to a temperature difference has been studied. The next step is to take into account the configuration of the heat exchanger used to extract this geothermal potential, as well as the different heat flows involved, since the tunnel is a hollow cylinder.

## 3.3 Results validation

The validation of the results here primarily involves confirming the trend and assessing the error introduced by this simplified method for estimating geothermal potential. Indeed, previous studies on tunnel geothermal systems have focused on 3D numerical models to predict the output temperature. Additionally, variations in ground temperature and soil type from site to site complicate direct validation of results.
In this context, the soil properties of Turin are used to evaluate the geothermal potential via the analytical solution, and the results obtained are compared with those obtained by Marco Barla through numerical simulation. Table 3.2 lists the soil properties: the undisturbed ground temperature is 14°C, which is 2°C higher than in the case study.

| Properties | Value | Unit |
|---|---|---|
| Porosity | 0.25 | – |
| Heat capacity of the water | 4.2 | $MJ/m^3/K$ |
| Heat capacity of the solid | 2.0 | $MJ/m^3/K$ |
| Thermal conductivity of the water | 0.65 | W/m/K |
| Thermal conductivity of the soil | 2.8 | W/m/K |
| Undisturbed ground temperature | 14 | °C |

Table 3.2: Thermal average parameters of the Torino subsoil.

Figure 3.8 illustrates the evolution of the geothermal potential over a 30-day period. The orange curve represents the solution obtained via the 3D model simulation, which takes into account the tunnel environment as well as the concrete lining in which the pipes are embedded. The blue curve, on the other hand, represents the result obtained using the simplified analytical method. It is visible that the two curves evolve in the same trend and remain almost parallel after 5 days. The potential estimated by the simplified analytical method is higher than that obtained via numerical simulation, which is the expected outcome. Indeed, the analytical solution does not account for the tunnel's internal environment or the various thermal resistances influencing heat transfer. The consistent difference, corresponding to an RMSE of approximately $47\,W/m^2$, between the two curves is therefore attributable to these neglected parameters, highlighting the need to model the heat exchanger while considering the different heat exchanges present.

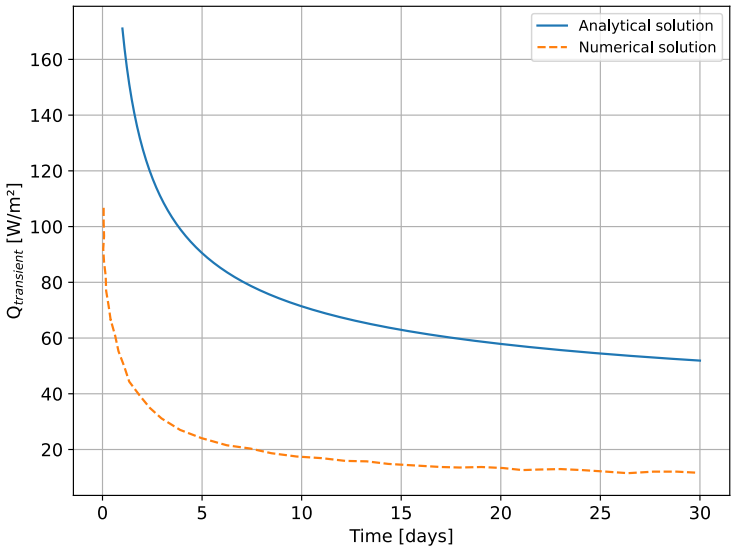


Figure 3.8: Evolution of heat potential for Turin soil.

Finally, the test carried out on Turin soil shows that the analytical solution overestimates the amount of heat exchanged between the ground and the tunnel, because it does not account for the various thermal resistances or the tunnel's internal environment. However, this simple method is very useful for comparing the geothermal potential of different soil types, as it provides an upper bound of the geothermal potential. The following chapter thus focuses on modelling the heat exchanger composed of polyethylene pipes embedded in concrete. This model is developed under the assumption that heat exchange occurs under steady-state conditions.

# Chapter 4

# Steady state evaluation of geothermal potential

Transient analysis makes it possible to determine the amount of heat transferred into the ground under a temperature gradient, particularly when a cylindrical surface is maintained at a constant temperature differing from that of the ground. However, in the context of an energy tunnel, this analysis does not take into account the various factors by which the temperature of the surface in contact with the ground is determined, namely, the tunnel's internal environment, the various thermal resistances that hinder heat exchange, the inlet temperature of the heat transfer fluid, etc. Moreover, the heat transfer fluid is carried through pipes that do not cover the whole surface of the lining. As a result, limits are placed on the amount of heat that can be collected, in addition to the physical constraints of heat exchange.
To take all these new factors into account, a steady state analysis is carried out. In this analysis, a heat exchanger model is proposed, in which the different thermal resistances and the various heat exchanges are taken into account. To carry out this analysis, the heat exchanger is first sized. Then, the model and its assumptions are described. Finally, sensitivity studies on certain model parameters are conducted, and the results obtained are validated.

## 4.1 Heat exchanger design sizing

As mentioned earlier, the tunnel under study is excavated using the TBM method. Thermal activation is therefore achieved by embedding Pe-Xa pipes into the lining, through which a mixture of propylene glycol and water, called heat transfer fluid, is circulated. The linings are prefabricated in a factory as segments, and depending on the tunnel diameter, several segments are assembled to form a lining ring. The heat exchanger, therefore, consists of pipes embedded within concrete segments, through which the fluid enters at one temperature ($T_{in,fluid}$) and exits at another ($T_{out,fluid}$), as shown in Figure 4.1. The fluid flowing through the thermally activated segment is heated by both the ground and the air inside the tunnel through the concrete. Thus, $Q_{air}$ denotes the amount of heat exchanged by convection with the tunnel's internal air, and $Q_{ground}$ denotes the amount of heat exchanged by conduction with the ground. The design of the heat exchanger involves determining the pipe dimensions and selecting the heat transfer fluid.

- **Configuration and dimensions of the heat exchanger**

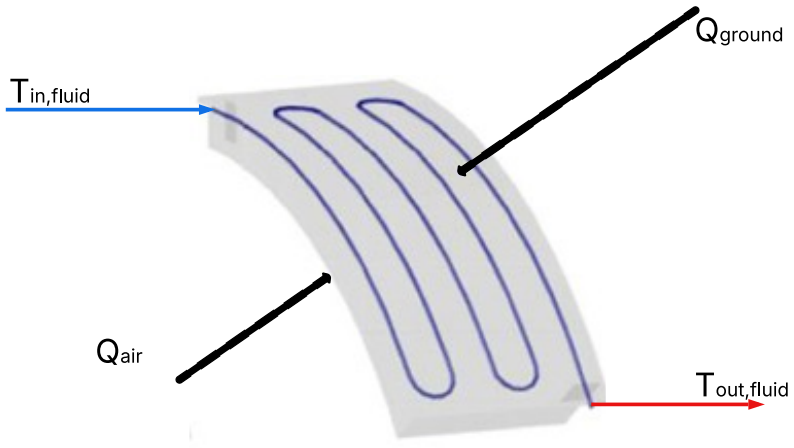


Figure 4.1: Configuration of Pe-Xa pipe, inlet/outlet fluid temperatures, and heat exchange

Figure 1.6b from Chapter 1, presented here as "Figure 4.1", is a schematic representation of the geometry of an ENERTUN profile of a thermally activated segment on the ground side. Based on the dimensions of the Liefkenshoek tunnel, the dimensions of the segment and the pipes are determined. Firstly, based on the tunnel dimensions (see Table 3.1), the perimeter of a lining segment is calculated, knowing that 7 are required to form a complete ring:

$$p_{segment} = \frac{\pi D_{out}}{7} = 3.64 \text{ m}$$

Next, based on the technical description of the ENERTUN prototype [25], the length of pipe per segment is estimated to be approximately 19 m. Table 4.1 summarises the sizing of a thermally activated lining segment.

| **Dimensions** | **Symbol** | **Value** | **Unit** |
|---|---|---|---|
| Pe-Xa Pipe position | $p$ | 40 | mm |
| Segment perimeter | $p_{segment}$ | 3.64 | m |
| Pe-Xa Pipe length | $l_p$ | 19 | m |
| Outer Pe-Xa pipe diameter | $d_e$ | 20 | mm |
| Pe-Xa Pipe thickness | $e_p$ | 2 | mm |

Table 4.1: Heat exchanger dimensions for one lining segment.

The segments thus sized are connected in series to form a loop, so that the fluid passes through the seven lining segments to exchange heat and exits at a given temperature, as shown in Figure 4.2. Thus, the total length of Pe-Xa pipe traversed by the fluid when completing a lining loop is $L_p = l_p \times 7 = 133$ m.

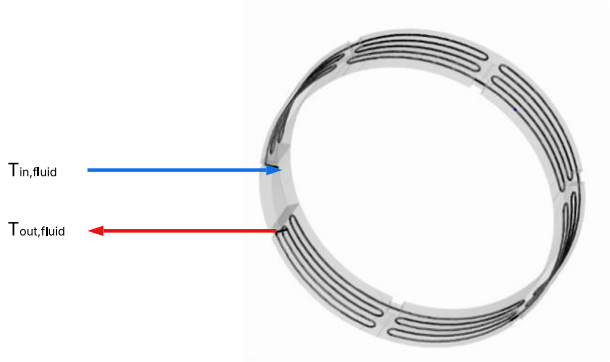


Figure 4.2: Representation of a thermally activated lining ring.

- **heat transfer fluid**
  The heat transfer fluid is a mixture of water and propylene glycol. Water alone represents the best heat transfer fluid due to its high specific heat capacity, low viscosity, and low cost. However, to prevent bacterial growth and the freezing of water, which occurs at 0°C in extreme conditions, propylene glycol is added to lower the freezing point and inhibit bacterial proliferation. An additional effect of this addition is the increase in the fluid's dynamic viscosity. In the design of the ENERTUN profile and related studies by Marco Barla, turbulent flow of the heat transfer fluid has been prescribed, as heat exchange is enhanced under these conditions due to mixing of fluid layers. Yet, higher dynamic viscosity requires an increased flow rate to maintain turbulence. Consequently, higher flow rates are required to achieve turbulent flow, which results in significant pressure drops and thus requires the use of larger pumps. Furthermore, higher velocities also lead to a lower outlet temperature, as will be demonstrated later.
  Figure 4.3 illustrates the evolution of the Reynolds number for various propylene glycol (PG) concentrations at 4°C. 0% represents pure water, while 10% denotes water with 10% propylene glycol by volume. The figure demonstrates that the turbulent regime ($R_e > 2300$) is reached more rapidly for lower viscosity fluids.

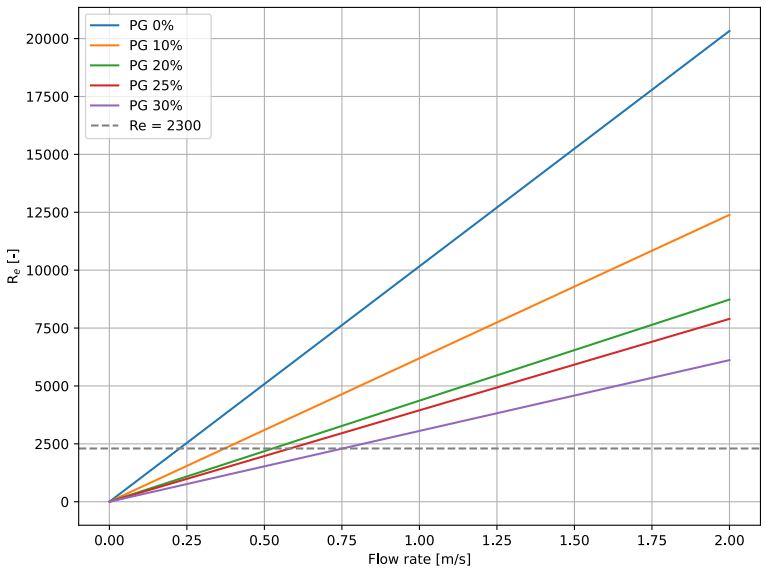


Figure 4.3: Reynolds number function of flow rate of the Heat-Transfer Fluid for Different Propylene Glycol Concentrations.

In conclusion, the heat transfer fluid must both maintain turbulent flow and sufficiently lower the freezing point according to operating conditions. Therefore, within this study, a 10 % concentration has been chosen. This concentration aligns well with Marco Barla's viscosity selection, ensuring a turbulent regime at 0.38 m/s.

With the heat exchanger sizing completed, the next step involves the development of an analytical model in which the various thermal resistances are represented. Then, the governing equations describing the heat exchanges are established, together with the working assumptions.

## 4.2 Description of the model and assumptions

The heat exchanger sized in the previous section is modelled using a thermal resistance network, as shown in Figure 4.4.

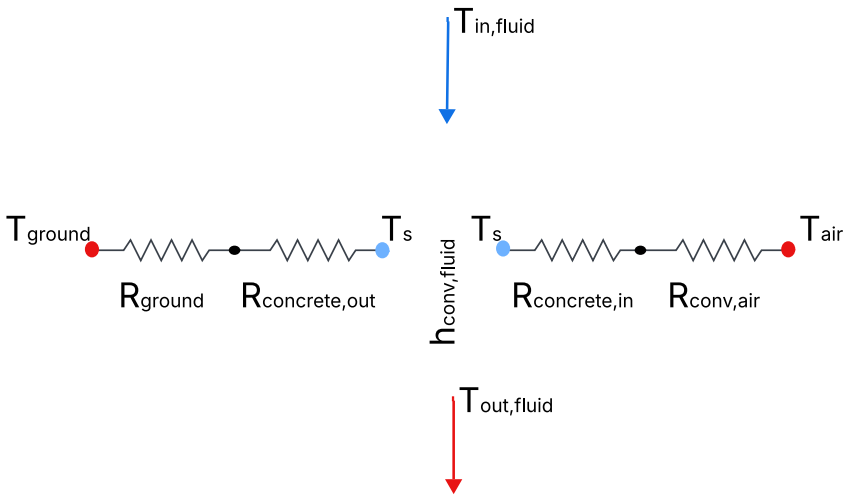


Figure 4.4: Thermal resistance heat exchanger diagram.

The heat exchanges taking place and their associated resistances are:

- The conduction heat transfer between the ground and the outer part of the lining is represented by $R_{ground}$, followed by the conduction between the concrete and the Pe-Xa pipe, represented by $R_{concrete,out}$.
- The convection heat exchange between the air flowing within the tunnel and the internal part of the lining is represented by $R_{conv,air}$, followed by the conduction between the concrete and the Pe-Xa pipe, represented by $R_{concrete,in}$.
- The Pe-Xa pipe is assumed to be sufficiently thin (2 mm in thickness) that the conduction resistance between the outer wall at temperature $T_s$ and the inner wall (also assumed to be at $T_s$) can be neglected. Therefore, only the convective heat exchange between the heat transfer fluid and the pipe's inner wall is considered, and is represented by $h_{conv,fluid}$.

From the previous sections, it was concluded that the potential assessed here concerns the use of urban heating with a heat pump. Consequently, the heat pump's performance must be evaluated. To this end, the heat exchanger model is complemented by a simple heat pump model, which is based on the calculation of the Carnot coefficient of performance.

Figure 4.5 presents the model of a heat exchanger directly integrated with a heat pump. The model is derived from the thermal resistance diagram and allows the classification of variables into inputs, outputs, and parameters.

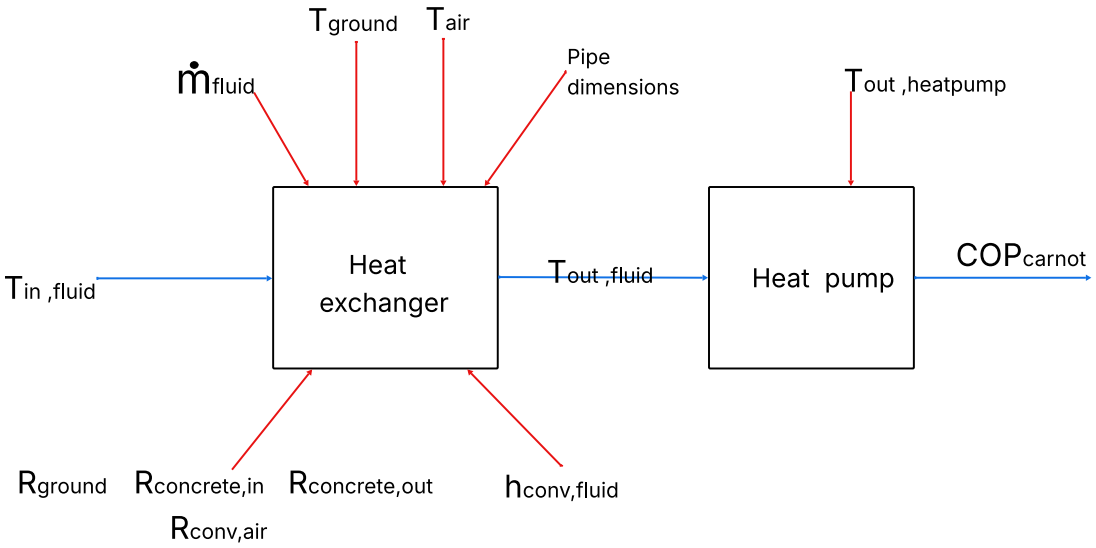


Figure 4.5: Heat exchanger model.

- Input and output
  - $T_{in,fluid}$: inlet temperature of the heat transfer fluid,
  - $T_{out,fluid}$: outlet temperature of the heat transfer fluid, which is the inlet temperature of the heat pump,
  - $COP_{carnot}$: Carnot COP of the heat pump.
- Parameters
  - $R_{concret,in}$,$R_{concrete,out}$: conductive thermal resistance of the tunnel lining,
  - $R_{conv,air}$: convective thermal resistance of the air inside the tunnel,
  - $R_{ground}$: soil conduction resistance,
  - $h_{conv,fluid}$: convective heat transfer coefficient of propylene glycol,
  - $\dot{m}_{fluid}$: flow rate of propylene glycol,
  - $T_{ground}$: ground temperature,
  - $T_{air}$: temperature of air inside the tunnel,
  - $T_{out,heatpump}$: outlet temperature of the heat pump.

The heat exchanger thus modelled, the resulting model and its equations (which are described in Section 4.3) can be solved. The use of this model to assess the potential is carried out under several assumptions, which are as follows:

- Steady state.
  The model is formulated under a quasi-steady assumption at the exchanger scale. The motivation is that the ground temperature field evolves on a much longer timescale than the fluid residence time and the conduction across the lining. Transient thermal effects in the ground are therefore neglected, and the far-field ground

temperature is fixed at 12°C while local gradients are represented through lumped resistances (in particular $R_{ground}$). The objective is to assess exchanger performance (extracted heat rate, outlet temperature, and the resulting Carnot COP of the coupled heat pump) under these steady boundary conditions. This assumption is consistent with numerical and analytical results that asymptotically approach a steady state under constant loads. Its limitation is that the slow drift of the ground (long-term depletion/recharge and any advective effects) is not captured; hence seasonal or multi-year behaviour must be evaluated with a transient framework.

- Uniform air temperature inside the tunnel.
  The tunnel air temperature is assumed uniform both along the axis and over the cross-section, and is fixed at 11°C. This simplification neglects axial advection of heat, stratification, and local sources/sinks associated with ventilation cycles and equipment; a constant convective coefficient is also adopted. Under this assumption, all thermo-active lining rings are predicted to exhibit identical performance, which may not hold under real operating conditions. The implication and potential bias of this assumption are addressed through a sensitivity analysis with respect to $T_{air}$(Section 4.4.3), which quantifies its effect on outlet temperature, extracted heat, and COP.

- The outlet temperature of the heat pump is fixed at 35°C. This value is established according to the application defined earlier, namely district heating with underfloor heating systems as heat emitters.

- The heat transfer fluid consists of water with 10% propylene glycol, which ensures turbulent flow even at low flow rates. In real systems, the heat transfer fluid contains between 20% and 40% propylene glycol, depending on the climatic conditions [26]. This assumption significantly reduces the impact of fluid viscosity on performance, and in practice, the flow may not remain turbulent.

- The inlet temperature of the fluid in the heat exchanger is fixed at 4 °C, which is the most commonly reported value in the literature. This assumption does not affect the validity of the model; it provides an initial reference value for performance evaluation. Subsequently, a sensitivity analysis will be performed to assess its impact on performance.

- About the flow rate in m/s or Kg/s, no fixed value is prescribed for it, as a sensitivity analysis will be conducted to identify the interval that ensures turbulent flow. It is therefore not treated as an unknown of the system.

- The convective heat transfer coefficient of the fluid is not fixed a priori, as its value depends on the inlet temperature and flow regime considered, but it is not treated as an unknown.

## 4.3 Model resolution

Once the heat exchanger model has been described, it must be solved. For this purpose, the various model parameters are calculated or specified; then, the governing mathematical equations for heat exchange are established; and finally, the model is solved.

### 4.3.1 Calculation of the model parameters

The following Figure illustrates more tunnel dimensions and the Pe-Xa pipes. The red ring represents the position of the pipes within the lining.

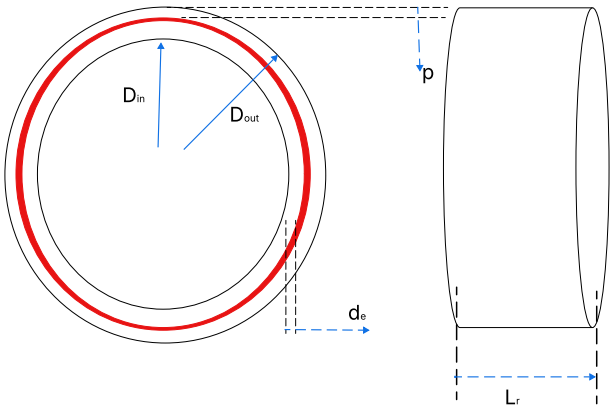


The parameters to be computed are: $R_{\text{ground}}$,$R_{\text{concret,in}}$,$R_{\text{concret,out}}$, $R_{\text{conv,air}}$,$h_{\text{conv}}$.

- $R_{\text{concret,in}}$,$R_{\text{concrete,out}}$
  The thermal resistance of the tunnel concrete lining is calculated on the inner side, in contact with the air, and on the outer side, in contact with the ground, depending on the position $p = 0.04$ m of the pipes carrying the heat transfer fluid. The calculation of the thermal resistance is carried out as follows, with $k_{\text{concrete}} = 2.3$ W/mK [11]:

$$R_{concrete,out} = \frac{\ln(D_{out}/(D_{out} - 2p))}{2\pi k_{concrete} L_r} \tag{4.1}$$

$$R_{concrete,in} = \frac{\ln((D_{out} - 2p - 2d_e)/D_{in})}{2\pi k_{concrete} L_r} \tag{4.2}$$

- $R_{ground}$
  The thermal resistance of the ground is calculated using a shape factor related to the geometry of the heat exchange between a semi-infinite medium and a cylindrical surface. This shape factor is given by the figure 3.5. Furthermore, considering that the tunnel largely passes through sand, the only soil type considered here is water saturated sand, assumed to have a thermal conductivity of $k_{\text{ground}} = 2.40$ W/mK.

$$R_{ground} = \frac{1}{S k_{ground}} \tag{4.3}$$

- $h_{conv}$, $\dot{m}_{fluid}$
  Heat transfer in the heat transfer fluid occurs by convection. The convection coefficient is calculated as follows:

$$h_{conv} = \frac{N_U k_{fluid}}{d_e - 2e_p} \tag{4.4}$$

$$R_e = \frac{\rho_{fluid} \mathrm{v} (d_e - 2e_p)}{\mu} \tag{4.5}$$

$$N_U = 3.66 \text{ if } R_e < 2300 \tag{4.6}$$

$$N_U = 0.023 R_e^{4/5} P_r^{0.4} \text{ if } R_e >= 2300 \tag{4.7}$$

$$P_r = \frac{c_p \mu}{k_{fluid}} \tag{4.8}$$

The chosen heat transfer fluid is 10% propylene glycol. Table 4.2 provides a summary of the thermophysical properties of the fluid as a function of temperature. These data will then be interpolated to determine the values corresponding to the selected inlet temperature.

| **T[°C]** | $\rho$ **[kg/m$^3$]** | $c_p$**[J/(kg·K)]** | $k_{fluid}$ **[W/(m·K)]** | **Dynamic Viscosity($\mu$) [mPa·s]** |
|---|---|---|---|---|
| -5 | 1012.96 | 4072.8 | 0.513 | 3.316 |
| 0 | 1012.42 | 4082.4 | 0.5158 | 3.022 |
| 5 | 1011.83 | 4064.4 | 0.5408 | 2.512 |
| 10 | 1010.94 | 4068 | 0.5468 | 2.07 |
| 15 | 1009.82 | 4071 | 0.5516 | 1.796 |
| 20 | 1008.48 | 4078.6 | 0.5564 | 1.52 |

Table 4.2: Thermophysical properties of propylene glycol at different temperatures.

The mass flow rate in Kg/s is calculated simply based on the fluid flow rate v in m/s, the pipe cross-sectional area, and the fluid density. The most commonly reported flow rates in the literature are 0.9 m/s, 0.7 m/s, and 0.4 m/s. For this study, a sensitivity analysis will be carried out over the range from 0.05 to 2 m/s.

$$\dot{m}_{fluid} = \rho_{fluid} \frac{\pi (d_e - 2e_p)^2}{4} \mathrm{v} \tag{4.9}$$

- $R_{conv,air}$
  Calculating air thermal resistance requires knowledge of the tunnel's air velocity. According to NFPA 502, the National Fire Protection Association (NFPA) recommends a minimum air velocity between 1.6 m/s and 2.5 m/s to prevent backlayering in the event of a fire. The interview with the tunnel maintenance team made it possible to set a maximum air velocity of 5 m/s inside the tunnel. The convective heat transfer coefficient of air is taken from an experimental study on concrete, which shows how this value evolves with the age of the concrete and under different air velocities [27]. For an air velocity of 4.3 m/s, the convective heat transfer coefficient for cured concrete at 20°C is approximately $h_{conv,air} = 6.9$ W/m$^2$K.

$$R_{conv,air} = \frac{1}{h_{conv,air}(\pi D_{in} L_r)} \tag{4.10}$$

| **Parameters** | **Unit** | **Value** |
|---|---|---|
| $R_{ground}$ | K/W | 0.01 |
| $R_{concrete,out}$ | K/W | 0.00038 |
| $R_{concrete,in}$ | K/W | 0.0034 |
| $R_{conv,air}$ | K/W | 0.0035 |
| $T_{out,heatpump}$ | °C | 35 |
| $T_{ground}$ | °C | 12 |
| $T_{air}$ | °C | 11 |

Table 4.3: Model parameters value.

Table 4.3 provides a summary of the model parameters,including both those that are computed and remain constant, and those that are prescribed. $T_{out,heatpump}$ is derived

from the definition of the application potential, which is district heating. $T_{air}$ and $T_{ground}$ are derived from assumptions and monitoring data from the Liefkenshoek tunnel site. Since thermal resistance represents the difficulty of a medium to transfer heat, the tunnel lining allows heat to pass through relatively easily.

### 4.3.2 Equations

The model involves using the logarithmic mean temperature difference (LMTD) method to determine the amount of heat extracted by the heat transfer fluid, reconciling the thermal fluxes from the ground and the air. The equations to solve the model are in Table 4.4.

$$R_1 = R_{concrete,out} + R_{ground}$$
$$R_2 = R_{concrete,in} + R_{conv,air}$$

| **Equation Name** | **Mathematical Expression** |
|---|---|
| (1)Heat flux from the ground | $Q_{\text{ground}} = \dfrac{T_{\text{ground}} - T_s}{R_1}$ |
| (2)Heat flux from the air | $Q_{\text{air}} = \dfrac{T_{\text{air}} - T_s}{R_2}$ |
| (3)Total convective heat flux | $Q_{\text{conv}} = Q_{\text{ground}} + Q_{\text{air}}$ |
| (4)Energy transferred to the fluid | $Q_{\text{conv}} = \dot{m}_{\text{fluid}} c_p (T_{\text{out,fluid}} - T_{\text{in,fluid}})$ |
| (5)Temperature difference at inlet | $\Delta T_{\text{in}} = T_s - T_{\text{in,fluid}}$ |
| (6)Temperature difference at outlet | $\Delta T_{\text{out}} = T_s - T_{\text{out,fluid}}$ |
| (7)Logarithmic mean temperature difference | $\Delta T_{\text{lm}} = \dfrac{\Delta T_{\text{out}} - \Delta T_{\text{in}}}{\ln\left(\frac{\Delta T_{\text{out}}}{\Delta T_{\text{in}}}\right)}$ |
| (8)Heat transfer surface | $A_{\text{lat}} = \pi d_e L_p$ |
| (9)Final convective relation | $Q_{\text{conv}} = h_{\text{conv}} A_{\text{lat}} \Delta T_{\text{lm}}$ |
| (10)Carnot COP | $COP = \dfrac{T_{\text{out,fluid}}}{T_{\text{out,heatpump}} - T_{\text{out,fluid}}}$ |

Table 4.4: Model equations.

Equations 1 and 2 represent the heat exchange between the Pe-Xa surface, maintained at constant temperature $T_s$, and, respectively, the ground and the air through the concrete. Equations 3, 4 and 9 correspond to the different expressions for the heat exchanged by convection between the heat transfer fluid and the Pe-Xa pipe. These three equations serve to reconcile the fluxes and the various temperatures involved. Although the inlet fluid temperature $T_{\text{in,fluid}}$ is not a parameter, it must be specified as a model inlet. Thus, the model consists of three unknowns ($Q_{conv}$, $T_s$, $T_{\text{out,fluid}}$) for three equations, namely:

$$Q_{conv} = \frac{T_{\text{ground}} - T_s}{R_1} + \frac{T_{\text{air}} - T_s}{R_2} \tag{4.11}$$

$$Q_{conv} = h_{\text{conv}} A_{\text{lat}} \frac{T_{\text{in,fluid}} - T_{\text{out,fluid}}}{\ln\left(\frac{T_s - T_{\text{out,fluid}}}{T_s - T_{\text{in,fluid}}}\right)} \tag{4.12}$$

$$Q_{\text{conv}} = \dot{m}_{\text{fluid}} c_p (T_{\text{out,fluid}} - T_{\text{in,fluid}}) \tag{4.13}$$

This system of equations can be solved directly, but the computation of the logarithm on a computer may introduce errors and instability. To address this, the system is transformed into two equations for two unknowns system by substitution as follows:

$$\dot{m}_{\text{fluid}} c_p (T_{\text{out,fluid}} - T_{\text{in,fluid}}) = \frac{T_{\text{ground}} - T_s}{R_1} + \frac{T_{\text{air}} - T_s}{R_2}$$

$$\dot{m}_{\text{fluid}} c_p (T_{\text{out,fluid}} - T_{\text{in,fluid}}) = h_{\text{conv}} A_{\text{lat}} \frac{T_{\text{in,fluid}} - T_{\text{out,fluid}}}{\ln\left(\frac{T_s - T_{\text{out,fluid}}}{T_s - T_{\text{in,fluid}}}\right)}$$

The two final equations of the model to be solved are as follows:

$$T_{\text{out,fluid}} = T_s - (T_s - T_{\text{in,fluid}}) \exp\left(-\frac{h_{\text{conv}} A_{\text{lat}}}{\dot{m}\, c_{\text{fluid}}}\right) \tag{4.14}$$

$$T_{\text{out,fluid}} = T_{\text{in,fluid}} + \frac{\frac{T_{\text{ground}} - T_s}{R_1} + \frac{T_{\text{air}} - T_s}{R_2}}{\dot{m}\, c_{\text{fluid}}} \tag{4.15}$$

### 4.3.3 Equations resolution

The final system of equations of the model (Equations 4.14 and 4.15) is established. This system is a first-degree linear equation system that can be solved using various Python modules.

$$eq_1 = T_{\text{out,fluid}} - T_s - (T_s - T_{\text{in,fluid}}) \exp\left(-\frac{h_{\text{conv}} A_{\text{lat}}}{\dot{m}\, c_{\text{fluid}}}\right) \tag{4.16}$$

$$eq_2 = T_{\text{out,fluid}} - T_{\text{in,fluid}} + \frac{\frac{T_{\text{ground}} - T_s}{R_1} + \frac{T_{\text{air}} - T_s}{R_2}}{\dot{m}\, c_{\text{fluid}}} \tag{4.17}$$

Equations 4.16 and 4.17 represent an alternative way of expressing the model's system of equations. The expressions eq1 and eq2 are residuals that are set to zero in a perfect model or, in this case, are simply to be minimised. Furthermore, the model presents various physical constraints, which lead to the selection of constrained optimisation by minimising the sum of the squares of the residuals. For this purpose, Python's scipy.optimize. minimize function is used. Figure 4.6 presents the algorithmic diagram of the optimisation procedure: this diagram shows the various calculation steps, the expression of the objective function, and the physical constraints imposed.
A simple description of the algorithmic diagram's steps, from top to bottom, is as follows:

- The parameters and inlet temperature are initialised.
- Residuals (eq1, eq2) and objective function are expressed based on the unknowns.
- Definition of the constraints.
- Initialisation of the unknowns.
- The constrained minimisation of the objective function is performed using SciPy's minimize module.
- The optimisation outcome is assessed. In case the optimisation is successful, the outlet fluid temperature and the pipe temperature are accepted. If not successful, the model parameters and the inlet temperature are reset, and the optimisation is retried.

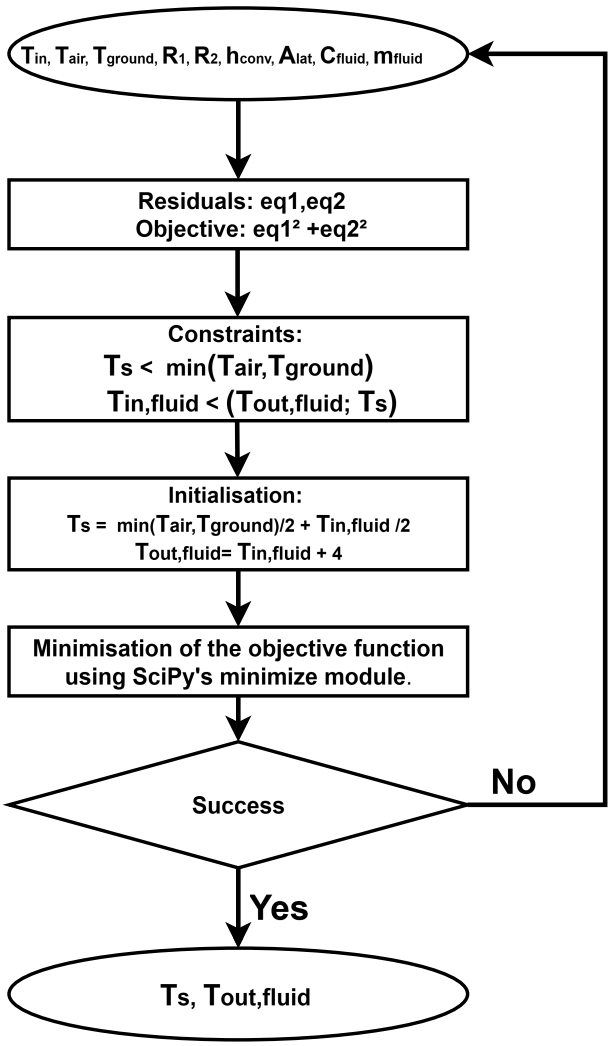


Figure 4.6: Algorithm diagram.

The description of the method used to solve the model has now been completed. The model may be deployed, and its results studied and compared. The issue previously mentioned stems from the lack of accurate measurements concerning both the soil properties and the tunnel's internal environment. Accordingly, sensitivity studies are performed on the model to assess the impact of certain model parameters and the inlet temperature of the heat transfer fluid on its performance. These results will be compared with those from other studies, in order to validate the model.

## 4.4 Sensitivity analysis and validation of the results

The performance indicators of the modelled heat exchanger include the Carnot COP of the heat pump and the extracted heat quantity, both of which are influenced by the exchanger's outlet temperature, as shown in line 10 of Table 4.4. Furthermore, according to Equations 4.14 and 4.15, the outlet temperature is influenced by the heat transfer fluid's flow rate, the internal air temperature, the ground temperature, the fluid's inlet temperature, etc. In this study, only three sensitivity analyses are performed, namely the effects of the fluid flow rate, the inlet temperature of the heat transfer fluid, and the internal air temperature within the tunnel.

### 4.4.1 Sensitivity analysis on the flow rate of the fluid in the heat exchanger.

The first sensitivity analysis focuses on the selection of the heat transfer fluid flow rate. Equations (4) in Table 4.4 and equation 4.14 show that the mass flow rate directly influences the outlet temperature of the heat exchanger and the amount of heat exchanged. The underlying physical quantity is the flow rate, making its selection a critical factor. A simple approximation allows for the calculation of the residence time of the fluid in the heat exchanger using the relation $t = \frac{L_p}{v}$ with $L_p$ the path length in m and v is the flow rate in m/s. Therefore, the lower the velocity, the longer the residence time in the exchanger. As stated earlier, the choice of heat transfer fluid was made to ensure turbulent flow, and the sensitivity analysis over a 0.05 to 2 m/s range and $T_{in,fluid} = 4°C$ shows that heat exchange is more effective under turbulent conditions, which is evident as the outlet fluid temperature approaches the pipe wall temperature $T_s$.
Figures 4.7a and 4.7d show the variation of the outlet temperature and the COP as a function of the fluid flow rate. Both the COP and the outlet temperature exhibit a similar trend, decreasing as velocity increases. In contrast, the amount of heat exchanged increases with fluid velocity. This behaviour represents the expected outcome, illustrating the trade-off between thermal efficiency (COP) and exchanged heat power.

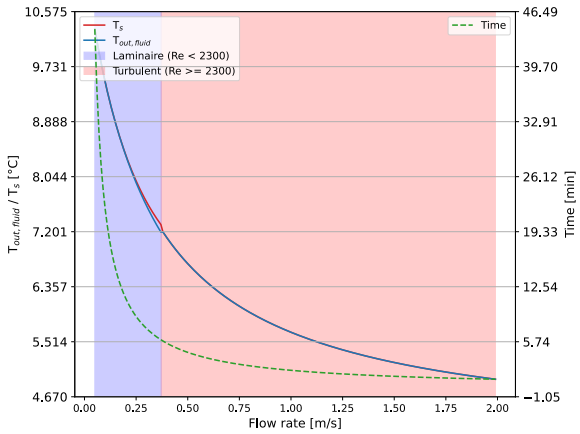


(a) Outlet heat exchanger temperature and time duration into the heat exchanger.

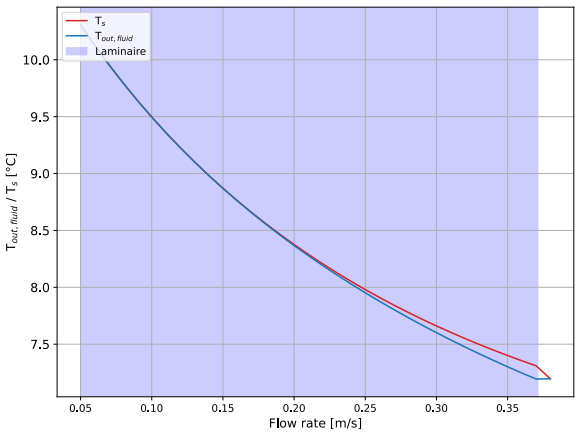


(b) Zoom 1.

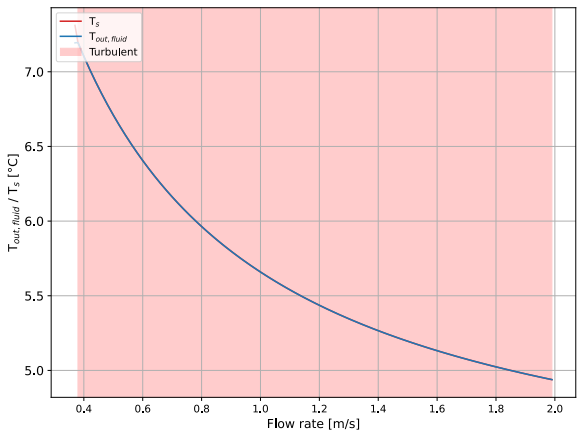


(c) Zoom 2.

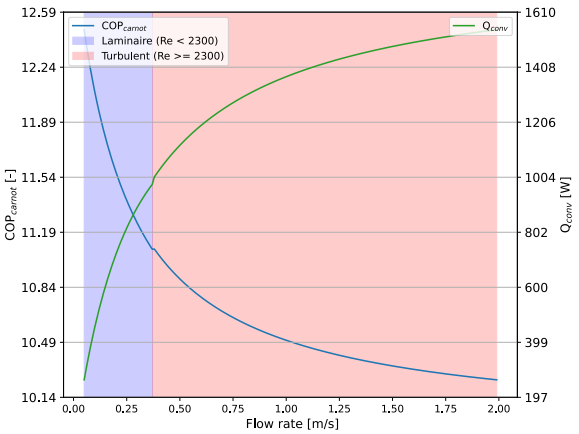


(d) Carnot COP and the heat potential.

Figure 4.7: Evolution of the outlet heat exchanger temperature, the Carnot COP, and the heat potential as a function of the fluid flow rate.

At low flow rates, the flow is laminar: the outlet fluid temperature remains close to the tube wall temperature due to the long residence time. As the flow rate increases, a difference develops between the two temperatures, as shown in Figure 4.7b. However, in turbulent flow, despite a shorter residence time, more efficient heat exchange brings the outlet fluid temperature close to the wall temperature once again (Figure 4.7c).
In the second part of this sensitivity study, a comparison is made between the results obtained and those from other works, along with the validation of the model. The evolution of the outlet temperature as a function of the flow rate, as obtained from the model, is presented in Figure 4.8a together with the results from numerical simulations performed using the FEFLOW software, within the framework of studies conducted on the Turin metro tunnel. A similar trend is observed for both curves, which become nearly parallel beyond 0.4 m/s. Below this velocity, the curves ares not parallel, as the model remains in the laminar regime, whereas at the same flow rate, the numerical simulation has already transitioned to the turbulent regime. This discrepancy is attributed to the use of different heat transfer fluids in the two cases. Regarding the value itself, considering the differences in ground types and various other factors, the values cannot be expected to be identical. Table 4.5 compares the parameters common to the numerical simulation conducted on the Turin tunnel and the analytical model developed in this study.

| **Parameters** | **Numerical modelling** | **Analytical model** |
|---|---|---|
| $T_{in,fluid}$[°C] | 4 | 4 |
| $T_{\text{ground}}$ [°C] | 14 | 12 |
| $T_{\text{air}}$ [°C] | 13.1 | 11 |
| Tunnel Diameter [m] | 7.4 | 8.10 |
| Lining ring axial length[m] | 1.4 | 1.8 |
| Pe-Xa pipe diameter [mm] | 25 | 20 |
| Fluid viscosity [mPa.s] | 1.7 | 2.61 |

Table 4.5: Comparative summary of Turin numerical modelling and the Analytical model.

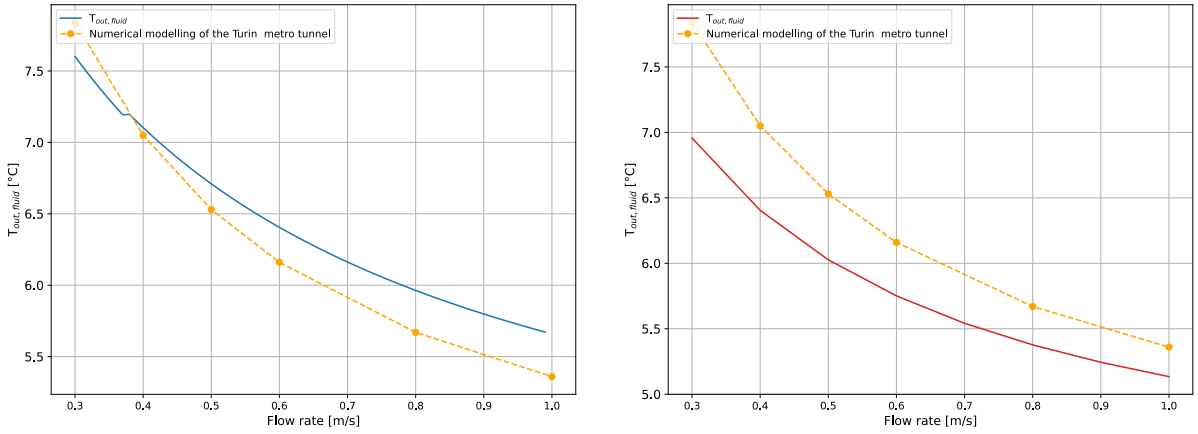


(a) Validation of the curve trend.

(b) Validation of the analytical model.

Figure 4.8: Comparison of outlet heat exchanger temperature.

The validation of the model is carried out here by testing it with the identified common parameter values. The red curve in Figure 4.8b illustrates the evolution of the outlet fluid temperature as obtained from the model. A similar trend is exhibited by the numerical

simulation curve. The discrepancy between the two curves can typically be attributed to the fact that the numerical simulation accounts for several additional factors; specifically, underground flow, more complex heat exchange mechanisms, and a heat carrier fluid whose properties are not explicitly defined. However, the root mean square error (RMSE) observed between the two curves amounts to 0.44 K, which is significantly lower than the RMSE of 47 $W/m^2$ obtained when using the analytical solution in transient conditions. This indicates that the analytical model in steady state aligns with the numerical simulation with an accuracy of 0.54 K. Such performance enables a concluding validation of the model and its derived results. Therefore, the model may be employed for a preliminary assessment of the exploitable geothermal potential in a feasibility study involving thermal activation of tunnels.
Finally, the purpose of the sensitivity study is to determine the impact of flow velocity on the exchanger's performance, specifically to identify a velocity range that optimises heat transfer. The transition from the laminar to the turbulent regime occurs at approximately 0.380 m/s. Consequently, the flow velocity should exceed this threshold, but not become excessively large, as an excessively high velocity brings the outlet temperature too close to the inlet temperature, thereby reducing the Carnot COP. Moreover, excessively high flow velocities significantly increase pressure losses (head loss) in the circuit, requiring more powerful and costlier pumps. Therefore, the valid velocity interval is established between 0.380 and 1 m/s, a range that aligns well with the values commonly recommended in the literature.
For the remainder of the study, a flow rate of 0.70 m/s was selected, as it ensures operation in the turbulent regime regardless of the temperature (higher viscosity at lower temperatures). This also enables the achievement of a thermal potential of 1252 W per ring, corresponding to approximately 695 W/m or 27 $W/m^2$ and a Carnot COP of 10.7 for an inlet temperature of 4°C.

### 4.4.2 Sensitivity analysis on the inlet temperature of the fluid in the heat exchanger.

The previous sensitivity study enabled validation of the fluid velocity range; a flow velocity of 0.70 m/s was adopted for the remainder of the analysis. This phase also validated the model by confirming the consistency of the outlet temperature evolution, and, consequently, the evolution of the coefficient of performance (COP) and the amount of heat exchanged.
Another significant parameter that affects heat transfer is the inlet fluid temperature. Indeed, conductive heat transfer becomes more pronounced when the temperature gradient is large (the greater the difference between the fluid and the surrounding medium, the higher the heat flux), as described by Fourier's law, as illustrated in Figure 4.9b. However, Figure 4.9a shows that the outlet temperature of the heat exchanger will also be lower, resulting in a lower Carnot COP. Here, the observed variations are much greater, highlighting the significant impact of this factor on the amount of heat extracted.

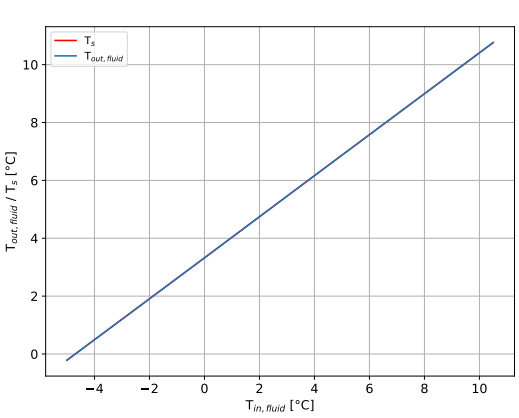


(a) Outlet heat exchanger temperature.

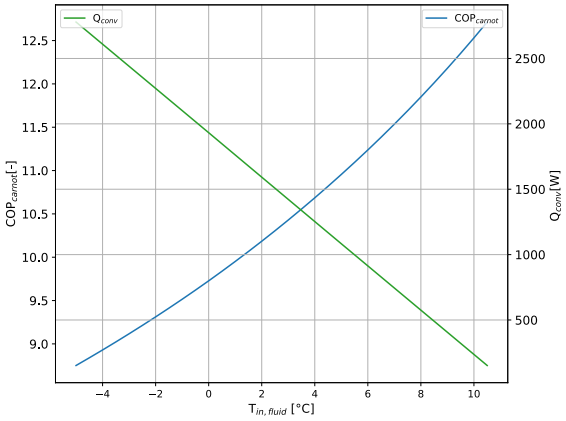


(b) Carnot COP and the heat potential.

Figure 4.9: Evolution of the outlet heat exchanger temperature, the Carnot COP, and the heat potential as a function of the inlet heat exchanger temperature.

Once again, there is a trade-off between the heat pump's performance and the thermal potential. The nearly linear evolution of the outlet temperature, the coefficient of performance, and the amount of heat exchanged with respect to the inlet fluid temperature is fully consistent with expectations.

### 4.4.3 Sensitivity analysis on the tunnel inside air temperature.

This latest sensitivity study focuses on the inside air temperature of the tunnel. It represents a way to investigate the impact of the tunnel's internal environment on the thermal performance of the heat exchanger. By varying the air temperature between 7 and 16°C, Figure 4.10a shows that the outlet temperature of the heat exchanger increases with the air temperature inside the tunnel. Consequently, the Carnot COP also increase. Furthermore, Figure 4.10b shows that the heat contributed by the air becomes increasingly significant compared to that from the ground as the temperature rises. In this case, the tunnel's internal environment has a greater impact on heat transfer than the ground. Therefore, for hot tunnels, the heat exchanger should be located on the air side. Once again, the observed linear trend is as anticipated.

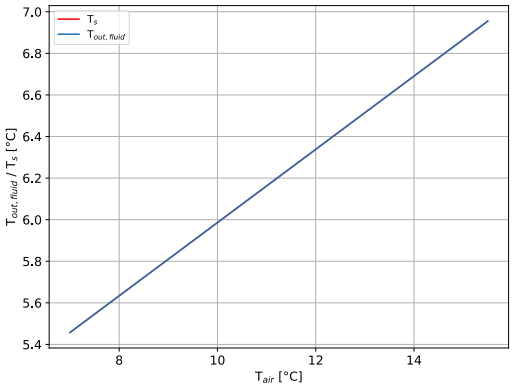


(a) Outlet heat exchanger temperature.

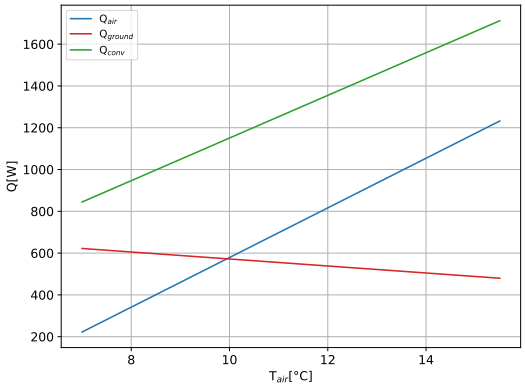


(b) Air and ground heat potential.

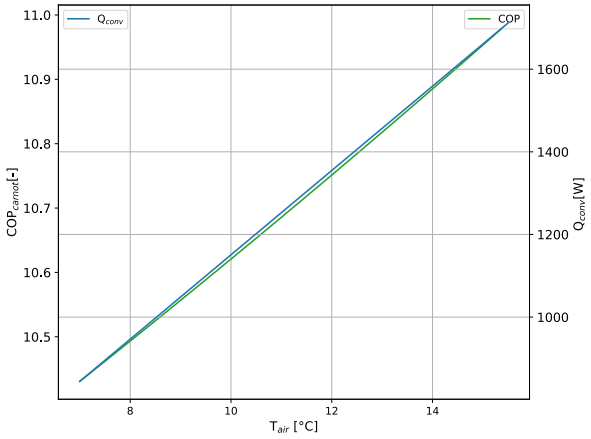


(c) Carnot COP and the heat potential.

Figure 4.10: Evolution of the outlet heat exchanger temperature, the Carnot COP, and the heat potential as a function of the inside tunnel air temperature.

In summary, the sensitivity analysis enabled the assessment of the influence of the fluid flow rate, inlet temperature and the air temperature inside the tunnel. This sensitivity study determined that a velocity range of 0.380 to 1 m/s is viable for a 10% propylene glycol-based heat transfer fluid, as it ensures turbulent flow while keeping pressure losses minimal. Furthermore, the model was validated in two ways: (1) by comparing the shapes of the curves obtained with those reported in the literature, and (2) by using the model with data from another study and comparing the results with the numerical simulation outputs of that study. For the remainder of sensitivity study, an approximately linear evolution was observed between the outlet temperature, coefficient of performance, and heat exchanged, on the one hand, and both the inlet fluid temperature and the tunnel's internal air temperature, on the other hand.
In the continuation of this study, the effect of flow velocity will be briefly presented based on results from other studies, to assess the impact of advection, as discussed in Chapter 3, on the exploitable geothermal potential.

## 4.5 Effect of groundwater flow

The effect of water flow in the soil results in heat transport by advection. Analytically, the flow velocity is taken into account through the calculation of an effective thermal conductivity in the three directions, and the total thermal conductivity is then the product

of these values, as follows:

$$k_x = k_m + \alpha_l \rho_w c_w u_x \tag{4.18}$$
$$k_y = k_z = k_m + \alpha_t \rho_w c_w u_x \tag{4.19}$$
$$k_e = k_x \times k_y \times k_z \tag{4.20}$$

Where $u_x$ is the flow velocity in the soil, $\rho_w$ is the density of water, $c_w$ is its specific heat capacity, $k_m$ is the thermal conductivity of the medium without groundwater flow, and $\alpha_{l(t)}$ is the longitudinal (transverse) dispersivity. Coefficients $\alpha_l$ and $\alpha_t$ are determined empirically and are always non-negative. The global analytical effect of groundwater flow is an increase in the effective thermal conductivity of the medium. As shown in Section 3.2.4, the higher the thermal conductivity, the greater the available thermal potential. Furthermore, the Darcy velocity q, which is used in the advective term of heat transfer, can be used for simulation in a 3D software environment. Figure 4.11 shows the effect of flow velocity on the influence zone of a borehole heat exchanger after 1 year of extraction. These results are derived from a numerical 3D simulation study conducted using FEFLOW software, focusing on the effect of the soil's thermal properties, as well as those of the borehole heat exchanger itself, on its performance [21].

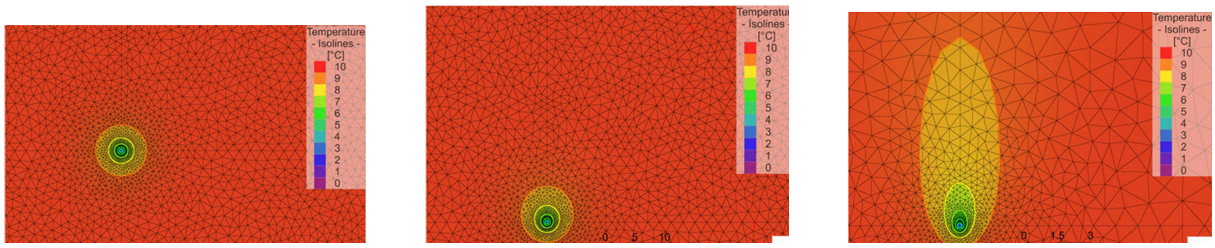


(a) $q = 10^{-9}$ m/s (b) $q = 10^{-7}$ m/s (c) $q = 10^{-6}$ m/s

Figure 4.11: Influence zone of the borehole heat exchanger for various groundwater flow velocities.

It can be observed that the greater the flow, the narrower the influence zone. However, this zone extends more downstream than upstream in the flow direction. Therefore, there is significant overall heat dispersion and dilution, which contributes to the thermal recharge of the ground and supports good long-term performance. This result also suggests that, in the present case study involving a twin tunnel located 15.6 m away and with groundwater flow perpendicular to the tunnel axis, the tunnel that meets the underground flow first will perform better than the second.
The experimental study conducted on the Turin metro pilot project, where two thermally activated lining rings were installed and tested, enabled the development of charts clearly illustrating the evolution of exploitable geothermal potential as a function of groundwater flow velocity [12]. The experimental study utilised in-situ measurements to calibrate a numerical simulation model in the FEFLOW software and generalised its findings to other soil types by representing them in terms of effective thermal conductivity.
Figure 4.12 is a reconstruction of t charts obtained under the assumption of groundwater flow perpendicular to the tunnel axis. This assumption is considered valid in n the case of the Liefenshoek tunnel, as the tunnel connects the two banks of a river. It shows the exploitable thermal potential per unit surface area of the tunnel as a function of the groundwater flow velocity and ground temperature.

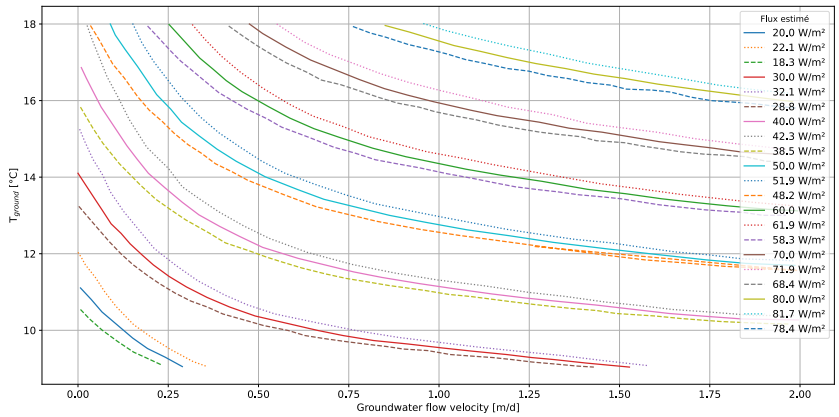


Figure 4.12: Thermal potential evolution as a function of groundwater flow velocity and ground temperature.

The solid line represents a soil thermal conductivity of 2.26 W/mK, the dashed line a conductivity of 3.9 W/mK, and the dotted line a conductivity of 0.9 W/mK. The effect of groundwater flow, which increases the amount of extractable heat, is observable. Furthermore, at 12°C, for a soil with thermal conductivity of 0.9 W/mK, ground temperature of 12°C and without groundwater flow, heat carrier fluid flow rate of 0.9 m/s and inlet temperature of 4°C, the thermal flux is 22 W/m$^2$. Under identical conditions, for saturated sand with a thermal conductivity of 2.40 W/mK, the analytical model yielded a geothermal potential of 29 W/m$^2$, which is higher than the 22 W/m$^2$ estimated for a soil with lower conductivity, as expected. However, this value remains lower than that predicted by the transient analytical solution, thereby confirming once again that the transient formulation overestimates the exploitable geothermal potential.

To conclude the assessment of the exploitable potential through thermal activation of the Liefkenshoek tunnel, the steady-state evaluation can be considered an appropriate approach for preliminary feasibility studies. Nevertheless, such studies alone are not sufficient to justify the initiation of a large-scale project. For this reason, Chapter 6 introduces an experimental protocol that compiles the steps required to progress from preliminary assessments to a pilot project, and, if feasible, towards full-scale implementation. Table 1 provides a synthesis of the thermal potentials reported for other energy tunnels in Europe.

| **Case study** | **Heat potential [W/m$^2$]** |
|---|---|
| Crossrail | 10–30 |
| Grand Paris Express A | 15–30 |
| Grand Paris Express B – case 2.1 | 50 |
| Jenbach | 18–40 |
| Katzenberg tunnel | 17–25 |
| Turin ML1 SE | 53 |

Table 4.6: Geothermal potential from other energy tunnel case studies.

As a reminder, the geothermal potential of the case-study tunnel was estimated to lie between 27 and 29 W/m$^2$ for a heat transfer fluid flowing at velocities between 0.7 and 0.9 m/s within the heat exchanger. In light of the results obtained for other European tunnels, it can therefore be concluded that the Liefkenshoek tunnel possesses a significant exploitable potential and may play a role in supporting the energy transition.

# Chapter 5

# Economic feasibility

Chapter 4 presented a study on the amount of heat that can be extracted through the activation of a lining loop, resulting in 1252 W of thermal output per 1.8 m of tunnel activation and a Carnot COP of 10.7 (heat transfer fluid flow rate of 0.7 m/s and inlet temperature of 4°C). That was a technical feasibility study. The focus now is to conduct an economic feasibility study. The possible application, namely district heating through a heat network, naturally emerges from the type of geothermal energy involved, which is low-enthalpy geothermal energy. Thus, the assumptions underlying this study are as follows:

- The length of the thermally activated tunnel is 6.10 km (3389 rings), corresponding to the deepest section of the tunnel,
- The exploitable potential is assumed to be the same along the entire length considered, regardless of the geostructure involved, and there is no interaction between the different lining ring,
- The district heating network includes a single large heat pump (centralised production).

To carry out this assessment, a non-exhaustive list of the steps required for the implementation of a shallow geothermal project is presented. From this list, the steps relevant to a tunnel lining thermal activation project are identified. Subsequently, the cost of heat production through tunnel thermal activation will be evaluated and compared with that of other heat production systems. The evaluation of this cost will be carried out within the framework and under the conditions of the sensitivity study on the inlet fluid temperature, to assess the impact of variations in the outlet fluid temperature on the cost of heat production.

## 5.1 Step for a shallow geothermal project

The first step is to determine the quantity of equipment required to thermally activate 6.10 km of tunnel, the total heat potential, the lifespan of the projet and the interest rate:

- Total heat power between 3 and 9 MW,
- Total length of PE-Xa pipes: $L_t = 450.7$ km,
- Total Length of Pe-Xa collectors pipes: $L_{\text{collector}} = 12.20$ km,

- The total flow rate of the heat transfer fluid is not taken into account, as the cost of the fluid is assumed to be negligible owing to its low propylene glycol content,
- The operating time is set to $\tau_e = 3500$ h/year, which is the value generally observed for geothermal systems,
- The operational lifespan of renewable energy systems is at least $N = 25$ years,
- In general, energy projects are financed by banks at interest rates ranging from 3% to $d = 5\%$. For the purposes of this study, an interest rate of 5% is adopted to represent the most conservative scenario. The interest rate serves as a measure of a project's real profitability, as it encompasses the cost of capital, risk, and the time value of money,
- Although the Enertun profile helps minimise pressure losses, a recirculation pump is still required. Pressure losses can be calculated using the Darcy-Weisbach equation:

$$\Delta P = f\frac{L}{D}\frac{\rho V^2}{2} \tag{5.1}$$

$$= 0.3164 R_e^{0.25}\frac{L_p}{d_e - 2e_p}\frac{\rho_{\text{fluid}}\text{v}^2}{2} \tag{5.2}$$

$$= 85.3 \text{ kPa} \tag{5.3}$$

The pressure losses per ring are approximately 85.39 kPa. Therefore, the pump must provide a minimum head of 8.6 m. The price range for such a pump is between €1,900 and 6800 € [28].

Table 5.1 provides a summary of the steps involved in a shallow geothermal project. In the case of energy tunnels, certain steps, such as drilling, can be bypassed by using existing structures [29] [30].

| **Stage** | **Estimated Cost** | **Tunnel Energy** |
|---|---|---|
| Preliminary study | 3,500 € – 9,000 € | Yes |
| Test drilling | 75 € – 113 € per meter | No |
| Feasibility study | 3,200 € – 5,800 € | Yes |
| Drilling and on-site connection Works | 70 € – 140 € per meter | No |
| Investment in heat pump | 195 € – 645 € per kW | Yes |
| Control and metrology system for heat Pump | 100 € – 430 € per kW | Yes |
| Installation of heat emitters | 12% – 67% of investment cost | Yes |

Table 5.1: Estimated costs of geothermal project development stages.

## 5.2 Assessment of investment capital, fix cost, and variable cost

This section presents an estimate of the capital investment required for a geothermal project applied to a tunnel. As a remainder, only the primary loop, that is the one on the geothermal heat exchanger side and heat pump, is considered in this study.

- Purchase and installation cost of equipment. Table 5.2 presents several equipment costs, with the highest prices being selected in order to represent the most disadvantageous scenario. The cost of electricity varies with the installed capacity, in this case ranging between 7 and 10 MW; as a result, it is included among the variable costs. By contrast, the cost of the heat pump control equipment also varies with installed capacity, but it is not treated as a variable cost; rather, it is added to the capital cost once the installed capacity is known.

| Equipment | Quantity | Unit cost | Total cost |
|---|---|---|---|
| $Pe-Xa$ pipes ⌀20 | 450.7 km | 34.30 €/ 25 m | 618411 € |
| $Pe-Xa$ pipes ⌀32 | 12.20 km | 136 €/ 50 m | 33184 € |
| Propylene glycol | / | / / | / |
| Pump | 2 | 6800 | 13600 € |
| Heat pump | / | / | 95000 € |
| Preliminary study | / | / | 9000 € |
| Feasibility study | / | / | 5800 € |
| Control and metrology system for heat Pump | / | 430 €/ kW | / |
| Electricity consumption for the heat pump | / | 0.059 €/kWh | / |

Table 5.2: Estimated total cost of equipment.

- The investment cost is approximately estimated at $C_0 = 774995 + 430 \times P_{\text{rated}} \times 1000$ €. The maximum value obtained is 4.82 M€,
- The fixed costs here include the maintenance costs of the heat pump, which is around $C_{\text{fix}} = 1800$ €/year according to the French Agency for Ecological Transition (ADEME),
- The variable costs are calculated using the following formula:

$$C_{\text{var}} = \frac{P_{\text{rated}} \times 1000 \times \tau_e}{COP} C_{\text{elec}}$$

  The maximum value obtained is 444,441€/year.

## 5.3 Evaluation of the total system cost and the cost of heat

The total cost of a system (TSC) is calculated using the following formula:

$$TSC = CAPEX + OPEX_{\text{fix}} + OPEX_{\text{var}} \tag{5.4}$$

where:

- $CAPEX$: initial investment cost,
- $OPEX_{\text{fix}}$: fixed operating cost,
- $OPEX_{\text{var}}$: variable operating cost.

Each of the terms mentioned above is calculated as follows:

- $CAPEX = C_0$,

- First, the annuity factor over the project's operational lifespan N is calculated as follows:

$$\psi = \frac{d}{1-(1+d)^{-N}}$$

Subsequently, the variable and fixed OPEX are divided by the cumulative discount factor because these are recurring costs paid annually. Dividing by this factor brings their value back to the present.

$$OPEX_{\text{fix}} = \frac{C_{\text{fix}}}{\psi}$$

$$OPEX_{\text{var}} = \frac{C_{\text{var}}}{\psi}$$

It is important to note that neither fixed costs nor variable costs include the price of primary energy, as the heat is freely extracted from the ground, effectively reducing this cost to zero.

The cost of heat (COH) is defined as the ratio between the system's total discounted cost and the amount of energy produced over one year, assumed constant. This value is also discounted using the annuity factor to reflect the present value of cost and energy flows over the project's lifespan.

$$COH = \frac{TSC}{\frac{P_{\text{rated}}\tau_e}{\psi}}$$

Now that the economic assumptions and formulas are established, the resulting curves as a function of $T_{out,fluid}$ can be analysed and discussed.
The highest observed TSC (Figure 5.1a) is approximately 11 M€, which represents only about 1/76 of the construction cost of the Liefkenshoek tunnel, estimated by the European Investment Bank to be 841 M€ [31]. Furthermore, the highest COH obseved here (Figure 5.1b) is approximately 24 €/MWh, which is considerably lower than the estimated heat selling price on district heating networks, at around 78.2 €/MWh [32]. Overall, heat is produced at a cost significantly lower than its current selling price, which endows the project with strong economic viability and long-term sustainability.

Figure 5.1a illustrates that the TSC decreases as the fluid outlet (or inlet) temperature increases. Indeed, although a higher inlet temperature also results in a higher outlet temperature, the overall thermal gradient is reduced, thereby lowering the amount of heat exchanged. This leads to a lower installed capacity, as confirmed by Figure 5.1b, which in turn results in a reduction in both capital expenditure and associated variable costs.

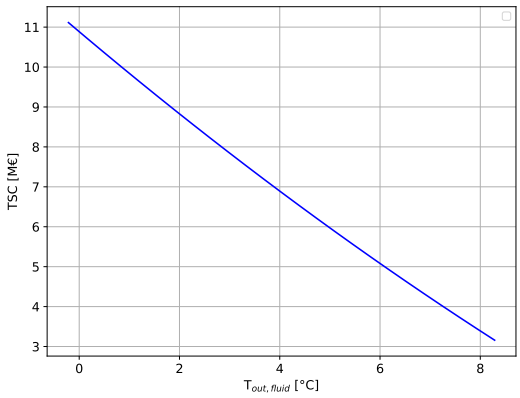


(a) Evolution of the system's total cost.

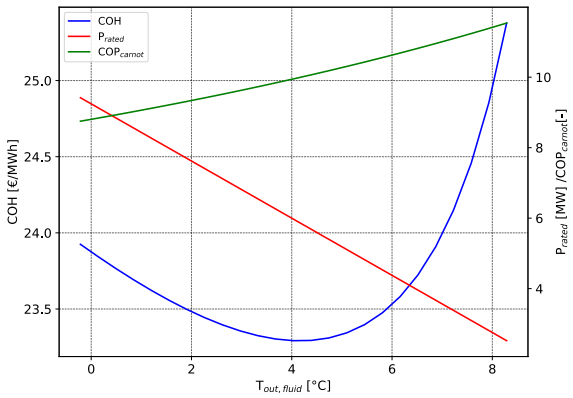


(b) Evolution of the cost of heat.

Figure 5.1: Evolution of the system's total cost and the cost of the heat as a function of the heat exchanger outlet temperature.

The COH, on the other hand, exhibits a completely different trend. Indeed, the cost decreases until the outlet temperature reaches around 4°C, which corresponds to an inlet temperature of approximately 1°C. Beyond this point, the heat cost begins to rise sharply. This phenomenon is simply due to the fact that the cost is levelised over the installed capacity. As long as the installed capacity remains relatively large, even if it decreases, the cost also diminishes. However, when installed capacity becomes too small, the fixed component of the investment cost remains high while the variable costs do not scale proportionately with the reduced capacity. Consequently, the heat cost ultimately increases.

In summary, although the Carnot COP increases with the fluid's outlet (and hence inlet) temperature, Figure 5.1 demonstrates that the critical determinant for both TSC and COH is the amount of heat collected by the heat exchanger. Accordingly, one can conclude that the fluid inlet temperature should be within the range of –2 to 4°C, and the outlet temperature within 2 to 6°C, so as to optimally balance COP, TSC, and COH. Now that the technical and economic feasibility of the thermal activation of the Liefkenshoek tunnel has been assessed, the next step is to propose an experimental protocol to transition from the feasibility study to a pilot project.

# Chapter 6

# Experimental protocol and perspectives

The preceding chapters enabled both technical and economic feasibility studies of geothermal potential for the Liefkenshoek tunnel case. This tunnel predominantly traverses water saturated sand layers. The transient analysis identified which soil types offer the highest geothermal potential, while the steady-state analysis quantified the heat exchanged through thermal activation of a lining loop, under various flow rates, inlet fluid temperatures, and internal tunnel air temperatures. It was concluded that the analytical steady-state model provides a valid preliminary estimation of the exploitable geothermal potential. It is important to note that this study, like many others, was conducted under various assumptions about soil properties and with several simplifications. This underscores the necessity of experimental pilot projects to validate, correct, or calibrate the models. Thus, this chapter presents a compilation of the steps to follow to move from the feasibility study to the implementation of a pilot project, and finally to a larger-scale deployment. Once these steps have been outlined, the resulting perspectives for future studies will be presented.

## 6.1 Experimental protocol

The experimental protocol proposed here assumes that the tunnel site has already been identified. The steps to be followed are:

- **Ground investigation**
  In the context of tunnel construction, geotechnical investigations are conducted to determine the soil composition and its properties from the surface down to tunnel depth. These studies generally establish the geological profile of the tunnel area; however, the physical properties (Porosity and void ratio, Degree of saturation, Deformation modulus, Grain-size distribution, etc.) measured are principally used to assess the mechanical and hydraulic behaviour of the soil. It is therefore proposed to supplement the standard geotechnical investigations with the evaluation of physical properties used to characterise the soil's thermal behaviour, namely: Temperature profile, thermal conductivity, specific (or volumetric) heat capacity, and thermal diffusivity.
  For an existing tunnel, the thermal properties of the surrounding soil can thus be determined through a Thermal Response Test (TRT), or alternatively based on measurements taken in areas adjacent to the tunnel. Section 3.2.1 presents an overview of different methods used to measure thermal properties.

- **Geothermal potential assessment**
  To evaluate the geothermal potential, the comprehensive study conducted here can

be applied as follows:

- Firstly, for a long tunnel, based on the properties of the geological layer in direct contact with the lining, the transient analytical solution can be used to determine the zones of the tunnel exhibiting the highest exploitable geothermal potential.
- Next, the heat exchanger should be modelled in steady state heat transfer, taking into account the tunnel geometry, the heat exchanger configuration, the heat transfer fluid, and simple heat exchange mechanisms (conduction and convection). The model developed in this study, considering only these heat transfer modes, achieves an RMSE of 0.54 K. It can be adapted to any tunnel shape other than a hollow cylinder by using the hydraulic diameter and the corresponding shape factor for the geometry used.
- A 2D or 3D model of the tunnel and the heat exchanger can be developed and simulated using software such as FEFLOW, COMSOL, or ANSYS. As illustrated in Figure 6.1, this model includes the surrounding ground, the internal tunnel air, the lining, and the Pe-Xa piping configuration inside the lining.

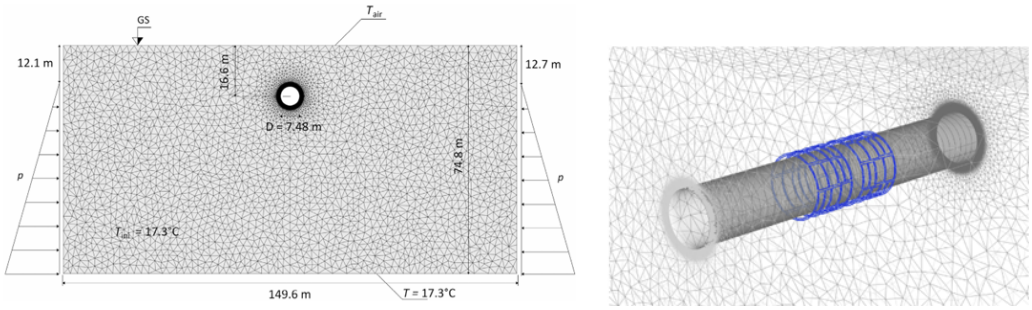


Figure 6.1: Example of a 3D model developed using FEFLOW

The use of 2D or 3D modelling, together with advanced simulation software, enables the consideration of complex heat transfer mechanisms, and can be further enhanced to incorporate distinct geological layers surrounding the tunnel. Numerical simulation requires a much broader set of soil properties compared to the simplified analytical model presented here. Consequently, it can be employed directly when all those properties are available. Moreover, it serves as a valuable tool to validate, correct, or calibrate the analytical model developed in the context of this study.

- **Pilot projet**
  Numerical simulation alone is insufficient to draw definitive conclusions on performance and to initiate a large-scale deployment; hence, the necessity of undertaking a pilot project on either an already constructed tunnel or a future tunnel. A pilot project allows for the implementation of a scaled-down system, the collection of real operating data, and the testing of the validity and reliability of analytical and numerical models before full-scale deployment. In other words, the experimental data collected at the pilot project site will be used to correct and calibrate the numerical models, which can then be extended to different operating conditions, such as a tunnel planned in a region other than the pilot site. As an illustrative example of a pilot project, the thermal activation of 2 to 5 lining loops—either in series or spread across multiple sections of the tunnel (whether under construction or

already completed)—is proposed. Initially, the thermally activated lining segments must be designed with the incorporation of sensors required for the experimental investigation. The ENERTUN profile currently stands as the most researched and effective configuration. These segments should then be installed in situ to enable data acquisition. The data required to assess thermal performance are divided into two categories: thermal performance indicators on the one hand, and structural mechanical performance metrics on the other. With regard to thermal performance, the data to be collected include: the outlet temperature, the flow rate, the inlet temperature of the heat transfer fluid, the air temperature inside the tunnel, and the ground temperature profile.

- **Full-scale deployment**
  Large-scale deployment represents the final stage of the project; however, it requires a comprehensive economic feasibility assessment. In particular, the heat extracted from the tunnel must be utilised in close proximity in order to minimise thermal losses during transport as well as the additional costs associated with pumping and reheating, consistent with district heating systems, where distribution losses typically amount to approximately 10%. Accordingly, a detailed analysis of the local heat demand surrounding the tunnel is required to define an appropriate extraction rate. Once this rate is established, the project's economic viability and long-term sustainability must be evaluated.

## 6.2 Perspectives

The preceding section on the experimental protocol has highlighted several future research directions regarding the feasibility of geothermal applications in deep Belgian tunnels, with the Liefkenshoek tunnel serving as a case study. As previously mentioned, if a pilot project exists, it can be used to calibrate numerical models that can be readily adapted for other Belgian tunnels. From this standpoint, the future perspectives are as follows:

- The study conducted here is based solely on a simplified analytical model. To verify the results and potentially calibrate this model, a 3D model and numerical simulation may be implemented.

- The study conducted here focuses solely on the recently constructed section of the tunnel, where the ground temperature remains constant at considerable depth. A feasibility study could alternatively be undertaken on the shallower sections of the tunnel, such as the cut-and-cover parts, by accounting for seasonal variations in ground temperature. This more complex analysis may be conducted via numerical simulation or by adapting the analytical model, provided that the seasonal temperature profile is available.

- The study presented here does not take into account the surrounding neighbourhood of the tunnel or its heat demands. A simple feasibility study could be conducted in this regard to identify the type of neighbourhood (residential, industrial, etc.) and assess whether implementing a geothermal solution in this area would be advantageous.

- Finally, the ultimate future direction is, of course, to execute a pilot project to validate and calibrate the models, thereby enabling the extension of the solution to other existing or planned tunnels, with the goal of large-scale deployment.

It should be noted that the structural feasibility study—aimed at assessing whether embedding a heat exchanger in the concrete lining compromises the integrity or primary function of the tunnel—is not presented here as a perspective, since it constitutes the subject of a separate master's thesis proposed by TUC RAIL. Nevertheless, it is directly embedded in the proposed protocol through the integration of dedicated sensors for this purpose.

This chapter closes the case study of the Liefkenshoek tunnel, covering aspects from its geometry to future perspectives. The following chapter sets out the general conclusion of this work.

# Chapter 7

# Conclusion

This master's thesis set out to assess the technical and economic feasibility of the thermal activation of the Liefkenshoek railway tunnel. To this end, a thermal modelling approach— combining analytical transient and steady state analyses— was developed, compared with findings from other European feasibility studies, and complemented by an economic assessment of profitability and sustainability.
The transient model showed that it tends to overestimate the exploitable geothermal potential. Nevertheless, it remains useful for identifying the most promising areas along the tunnel. The steady state model, which coupled the geothermal heat exchanger with a heat pump, estimated an exploitable potential of about $27\,\mathrm{W/m^2}$ when the fluid velocity in the exchanger is $0.7\,\mathrm{m/s}$ and the inlet temperature is 4°C. In addition, sensitivity analyses highlighted the influence of three key parameters: the flow rate, the inlet temperature of the heat transfer fluid, and the air temperature inside the tunnel. For the first two, a clear trade-off emerged between heat pump performance and the exploitable heat potential. The economic analysis confirmed the project's viability: with a maximum heat production cost on the order of 27 €/MWh, well below the current selling price observed on district heating networks (about 78 €/MWh), thermal activation of the tunnel can be considered economically attractive.
Overall, this work underlines how geothermal activation of existing infrastructure, particularly railway tunnels, can contribute both to the energy transition and to the energy valorisation of built structures. However, its experimental protocol emphasises that this energy must be utilised within the immediate vicinity: a neighbourhood study is essential, as well as a thorough economic analysis that accounts for the actual heat demand of the closest surrounding area, the proposed production system, and the means of heat distribution.
Looking forward, several perspectives arise. Firstly, it would be valuable to conduct numerical simulations to refine the analytical model results and to incorporate additional subsurface properties as well as complex heat exchange mechanisms not currently accounted for. Subsequently, an in situ pilot project on a section of the Liefkenshoek tunnel could be implemented to experimentally validate the expected performance and to calibrate the models for potential application to other tunnels in Belgium.

# Appendices

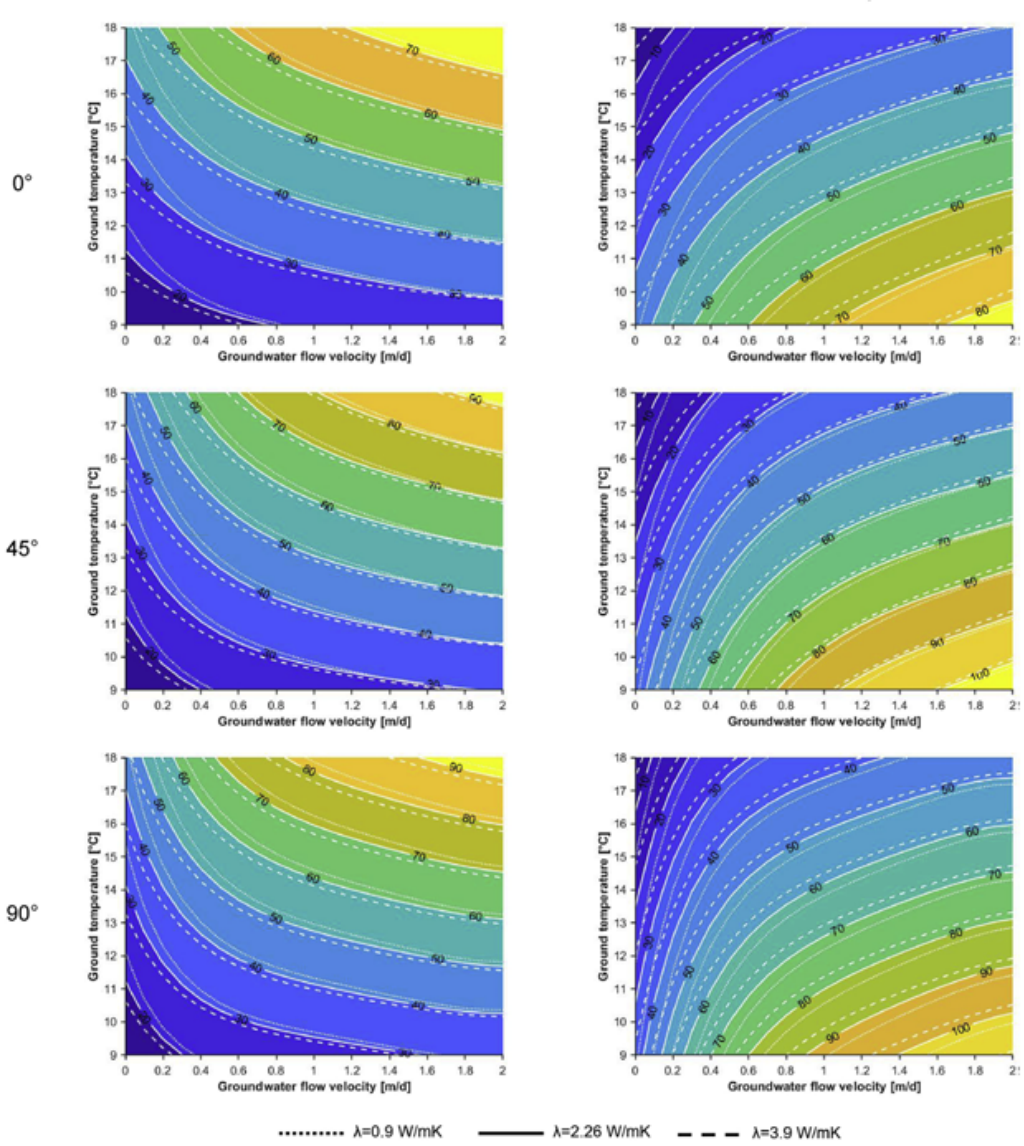


Figure 7.1: Diagram developed as part of the experimental study on the Turin tunnel[12].

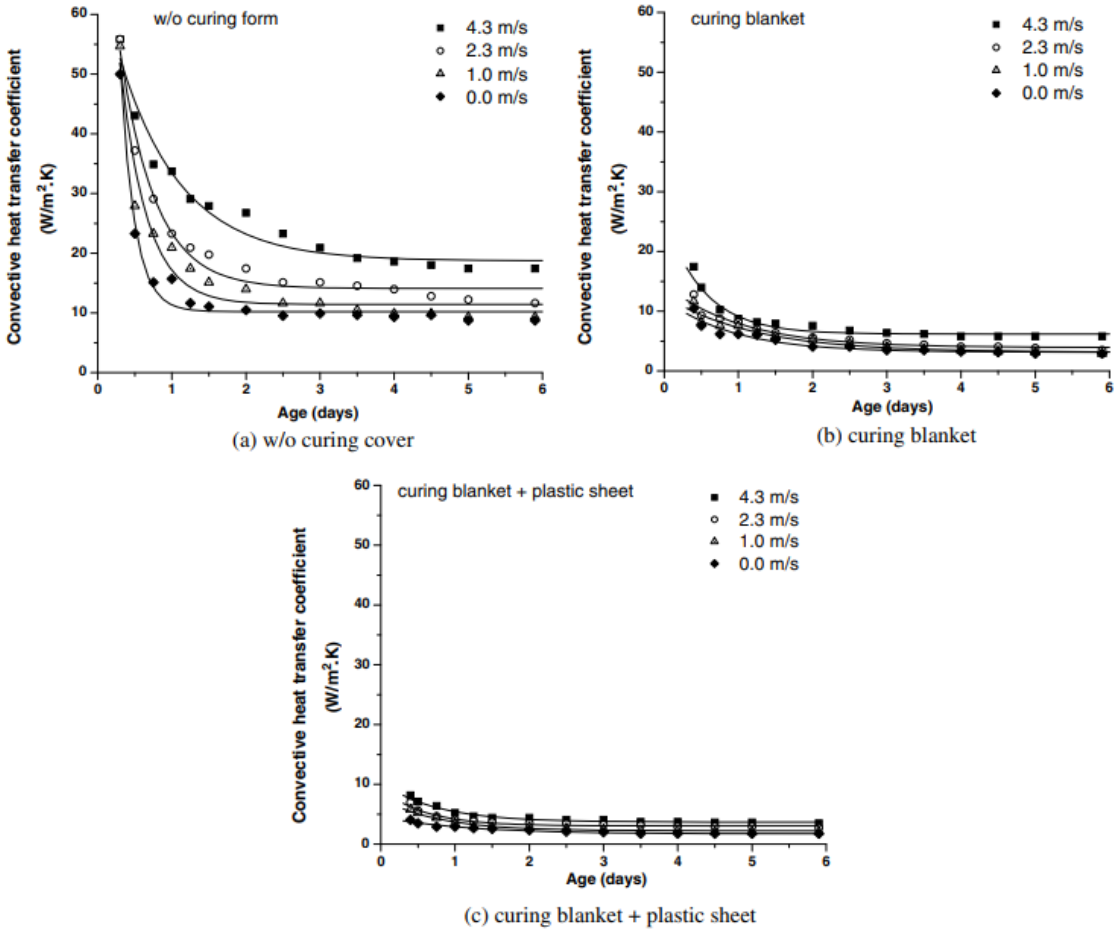


(a) w/o curing cover

(b) curing blanket

(c) curing blanket + plastic sheet

Figure 7.2: Evolution curve of the air convection coefficient on concrete as a function of concrete age [27].

# Bibliography


[1] Mireille Chiroleu-Assouline. *L'emploi et la transition énergétique*. Presses de Sciences Po, Paris, 2024. Chapitre 1.

[2] United Nations Framework Convention on Climate Change. The paris agreement. `https://unfccc.int/sites/default/files/english_paris_agreement.pdf`, 2015. Accessed: 2025-02-18.

[3] International Renewable Energy Agency (IRENA). Global energy transformation: A roadmap to 2050 - summary for policy makers. `https://www.irena.org/-/media/Files/IRENA/Agency/Publication/2018/Apr/IRENA_Global_Energy_Transformation_2018_summary_FR.pdf?la=en&hash=792E6F83EE4430DEE9C8B7424E09363A9B109547`, 2018. Accessed: 2025-02-18.

[4] European Environment Agency (EEA). Share of energy consumption from renewable sources. `https://www.eea.europa.eu/en/analysis/indicators/share-of-energy-consumption-from`, 2024. Accessed: 2025-02-18.

[5] Government of Belgium. Sources d'énergie et consommation durable en belgique. `https://www.belgium.be/fr/environnement/consommation_durable/sources_d_energie/energie`, 2025. Accessed: 2025-02-18.

[6] Alejandro García Gil, Eduardo Antonio Garrido Schneider, Miguel Mejías Moreno, and Juan Carlos Santamarta Cerezal. *Shallow Geothermal Energy: Theory and Application*, chapter Shallow Geothermal Systems with Closed-Loop Geothermal Heat Exchangers, pages 4–6. Springer Hydrogeology. Springer, Cham, 1st edition, 2022.

[7] Ingrid Stober and Kurt Bucher. *Geothermal Energy: From Theoretical Models to Exploration and Development*. Springer, second edition, 2021.

[8] Alice Di Donna. La géothermie, une source d'énergie verte sous nos bâtiments, 10 2019. Consulté le 12 mai 2025.

[9] Jannis Epting, Matteo Baralis, Rouven Künze, Matthias H. Mueller, Alessandra Insana, Marco Barla, and Peter Huggenberger. Geothermal potential of tunnel infrastructures – development of tools at the city-scale of basel, switzerland. *Geothermics*, 83:6–7, 2020.

[10] Ruben Stemmle, Kathrin Menberg, Ladislaus Rybach, and Philipp Blum. Tunnel geothermics–a review tunnelgeothermie–ein überblick. pages 105–107, 2022.

[11] Marco Barla, Alice Di Donna, and Andrea Perino. Application of energy tunnels to an urban environment. *Geothermics*, 61:104–105, 05 2016.

[12] A. Insana and M. Barla. Experimental and numerical investigations on the energy performance of a thermo-active tunnel. *Renewable Energy*, 152:781–792, 2020.

[13] Marco Barla, Alice Di Donna, and Andrea Perino. Application of energy tunnels to an urban environment. *Geothermics*, 61:104–113, 05 2016.

[14] Marco Barla, Alice Di Donna, and Alessandra Insana. A novel real-scale experimental prototype of energy tunnel. *Tunnelling and Underground Space Technology*, 87:1–14, 02 2019.

[15] Schotte, Ken and De Backer, Hans and Nuttens, Timothy and De Wulf, Alain and Van Bogaert, Philippe. Verification of the performance of the precast concrete lining in the Diabolo Tunnel and Liefkenshoek rail tunnel. In *IABSE conference : Assessment, upgrading and refurbishment of Infrastructures, Proceedings*, page 8. IABSE, 2013.

[16] Ken Schotte, Wim Nagy, Timothy Nuttens, Alain De Wulf, Philippe Van Bogaert, and Hans De Backer. Impact of tidal level fluctuations on the structural behaviour of a segmental tunnel lining. *Tunnelling and Underground Space Technology*, 64:184–208, 2017.

[17] Belgian National Stratigraphic Commission. Paleogene - neogene litho stratigraphy, 2023. Accessed: 2025-03-22.

[18] Centre Scientifique et Technique de la Construction. Note d'information technique n°259. Note d'information technique 259, Centre Scientifique et Technique de la Construction, December 2016. ISSN 0528-4880.

[19] Theodore L. Bergman, Adrienne S. Lavine, Frank P. Incropera, and David P. DeWitt. *Fundamentals of Heat and Mass Transfer*. John Wiley & Sons, Hoboken, NJ, 7 edition, 2011.

[20] Rendesco. Ground source heat pump networks, 2025. Accessed: 2025-06-01.

[21] S. Emad Dehkordi and Robert A. Schincariol. Effect of thermal-hydrogeological and borehole heat exchanger properties on performance and impact of vertical closed-loop geothermal heat pump systems. *Hydrogeology Journal*, 22(1):189–203, 2014.

[22] AGEO Luxembourg. Test de réponse thermique (trt), n.d. Consulté le 25 mai 2025.

[23] Precision Drilling Australia. What is a vibrating wire piezometer?, n.d. Accessed: 2025-05-25.

[24] Hot Dry Rocks. Portable electronic divided bar, n.d. Accessed: 2025-05-25.

[25] Alessandra Insana. *Thermal and structural performance energy tunnels*. Phd thesis, Université Paris-Est and Politecnico di Torino, 2020.

[26] CORECHEM Inc. Propylene glycol vs ethanol: A case for ethanol in geothermal systems. `https://corecheminc.com/propylene-glycol-vs-ethanol-a-case-for-ethanol-in-geothermal-systems/`. Accessed: 2025-08-20.

[27] Yun Lee, Myoung-Sung Choi, Seong-Tae Yi, and Jin-Keun Kim. Experimental study on the convective heat transfer coefficient of early-age concrete. *Cement and Concrete Composites*, 31(1):66–71, 2009.

[28] Industrial Pump & Equipment (IPEC) eStore. Ipec sales – estore, 2025. Accessed: 2025-06-01.

[29] Coûts de la géothermie très basse Énergie assistée par pompe à chaleur en hauts-de-france, données 2015-2019. Technical report, ADEME et Région Hauts-de-France, 2019. Accessed: 2025-06-01.

[30] Étude technico-économique de la géothermie de surface ,version 2020. Technical report, Association Française des Professionnels de la Géothermie (AFPG), 2020. Accessed: 2025-06-01.

[31] Banque européenne d'investissement. La bei finance un tunnel ferroviaire sous le port d'anvers, novembre 2008. Communiqué de presse n° 2008-104.

[32] Mona Guitou and Laurène Dagallier. Enquête sur le prix de vente de la chaleur et du froid en 2020. Série économique RCE 38, AMORCE, February 2022. Avec le soutien technique et financier de l'ADEME.